

An Analytic Theory of Near-Surface Relative Humidity over Land

KAIGHIN A. MCCOLL^{a,b} AND LOIS I. TANG^a

^a *Department of Earth and Planetary Sciences, Harvard University, Cambridge, Massachusetts*

^b *School of Engineering and Applied Sciences, Harvard University, Cambridge, Massachusetts*

(Manuscript received 7 June 2023, in final form 12 October 2023, accepted 1 December 2023)

ABSTRACT: There is no simple explanation for the spatial structure of near-surface relative humidity over land. We present a diagnostic theory for zonally and temporally averaged near-surface relative humidity (RH) over land based on energy budgets of an atmospheric column in radiative–convective equilibrium. The theory analytically relates RH to the surface evaporative fraction (EF), has no calibrated parameters, and is quantitatively accurate when compared with RH from a reanalysis, and with cloud-permitting simulations over an idealized land surface. The theory is used to answer two basic questions. First, why is RH never especially low (e.g., 1%)? The theory shows that established lower bounds on EF over land and ocean are equivalent to lower bounds on RH that preclude particularly low values, at least for conditions typical of the modern Earth. Second, why is the latitudinal profile of RH over land shaped like the letter W, when both specific humidity and saturation specific humidity essentially decline monotonically from the equator to the poles? The theory predicts that the latitudinal profile of RH should look more like that of water stored in the soil (which also exhibits a W-shaped profile) than in the air (which does not).

KEYWORDS: Humidity; Surface fluxes; Water budget/balance; Water vapor

1. Introduction

What determines relative humidity (RH) over land in the lowest few meters of the atmosphere? Many studies have considered RH in the free troposphere (Sherwood 1996; Pierrehumbert and Roca 1998; Held and Soden 2000; Dessler and Sherwood 2000; Sherwood and Meyer 2006; Sherwood et al. 2006; Pierrehumbert et al. 2008; O’Gorman and Schneider 2008; Sherwood et al. 2010a,b; O’Gorman et al. 2011; Romps 2014; Singh et al. 2019), or near an ocean surface (Held and Soden 2000; Schneider et al. 2010), and some have considered how it might change near a land surface in a warming world (Byrne and O’Gorman 2016, 2018). Yet, to our knowledge, there is no simple explanation for the structure of near-surface RH over land observed in the current climate. This is a significant knowledge gap: most humans and land plants spend most of their existence in the near-surface atmosphere, meaning near-surface RH directly impacts their health (e.g., Buzan and Huber 2020) and productivity (e.g., Berry et al. 2010).

This work begins the task of closing that knowledge gap by focusing on large-scale features of near-surface RH, relevant to the zonal and temporal average. Figure 1 shows near-surface RH over land in the ERA5 reanalysis (Hersbach et al. 2020). Hereafter, we will simply refer to “RH” instead of “zonally and temporally averaged near-surface RH.” Several questions arise, which are addressed in this study:

- Why is RH never especially low (e.g., 1%)? Over land, RH is typically never much lower than 35% (Figs. 1a,c). As noted in Romps (2014), this should be explainable in terms of basic physics given its ubiquity. However, the explanation given in Romps (2014), which is based on a simple model of a thermal plume rising through the free troposphere, is inapplicable near a land surface (more on this below). Similarly, RH over an ocean surface is typically always greater than $\sim 70\%$ (not shown), but is there any reason why it could not be much lower than this? What conditions, if any, would permit especially low values of RH?
- The latitudinal profile of RH shows a nonmonotonic pattern that resembles the letter W, with minima in the subtropics (Fig. 1c). What explains this pattern? At first glance, it may be tempting to attribute this to the fact that the tropics are generically “wet” and the subtropics are generically “dry.” But that explanation does not survive closer inspection. The same pattern is not present in the two atmospheric quantities most directly related to RH: specific humidity and saturation specific humidity. Both quantities essentially decrease monotonically from equator to pole (Fig. 1b). The W-shaped pattern cannot be explained, even qualitatively, solely in terms of variability in specific humidity (Fig. 1c, dashed blue line) or saturation specific humidity (Fig. 1c, solid blue line). The W-shaped pattern is, however, present in soil moisture (Fig. 10c). Why does the latitudinal profile of RH look more like that of water stored in the soil, than water stored in the near-surface atmosphere?

Previous theories that work well in the free troposphere are not easily transferable to near a land surface. Advection–condensation models are often used to understand relative humidity in the free troposphere (e.g., Dessler and Sherwood 2000; Pierrehumbert et al. 2008). In these models, an air parcel is advected by a given wind field. Water vapor in the air parcel is treated as a passive tracer that is only lost when condensation

 Denotes content that is immediately available upon publication as open access.

Corresponding author: Kaighin A. McColl, kmccoll@seas.harvard.edu

DOI: 10.1175/JCLI-D-23-0342.1

© 2024 American Meteorological Society. This published article is licensed under the terms of the default AMS reuse license. For information regarding reuse of this content and general copyright information, consult the AMS Copyright Policy (www.ametsoc.org/PUBSReuseLicenses).

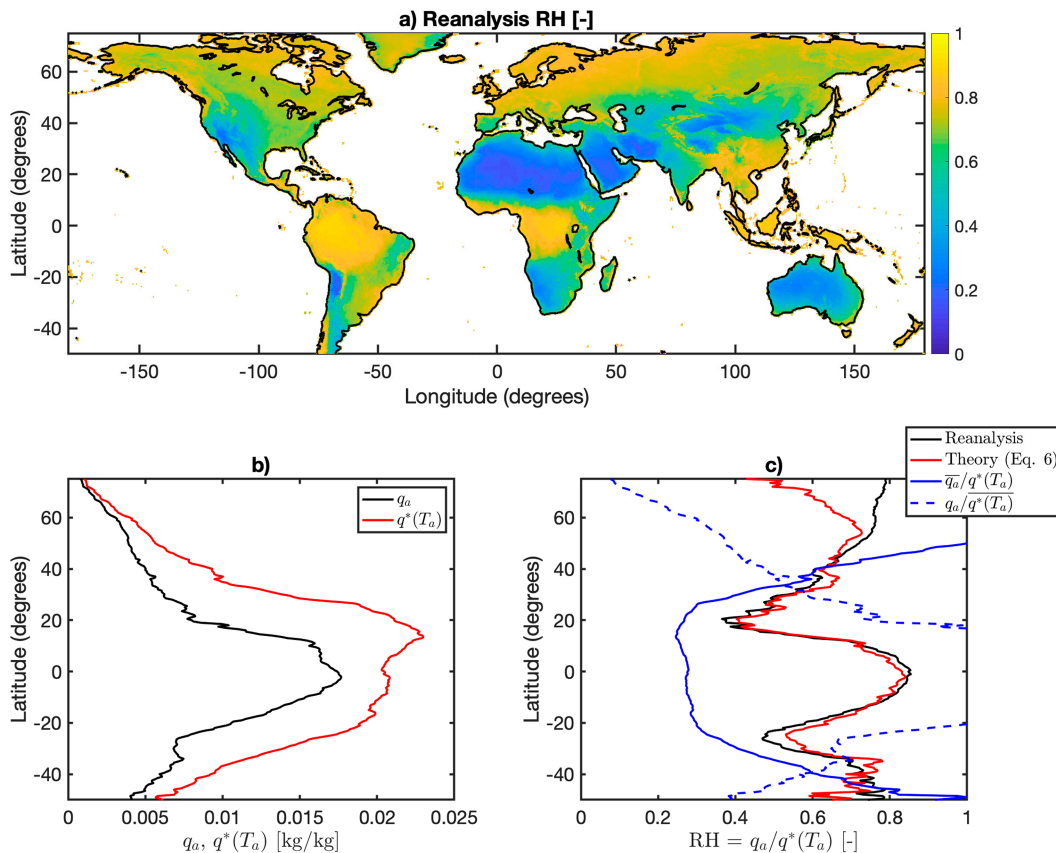


FIG. 1. (a) Global map of temporal median relative humidity in the ERA5 reanalysis over the period 1979–2021. Ocean is masked out (white regions). Zonal and temporal median (b) reanalysis specific humidity (q_a) and saturation specific humidity [$q^*(T_a)$] over land and (c) reanalysis RH over land and predicted RH over land from the theory proposed in this study [Eq. (6)]. For comparison with the theory, two alternative benchmarks are also shown in (c): the ratio of the global and temporal land median specific humidity (\bar{q}_a) to $q^*(T_a)$ (blue solid line) and the ratio of q_a to the global and temporal land median saturation specific humidity [$q^*(T_a)$]; dashed blue line]. Neither alternative reproduces the W-shaped pattern, even qualitatively.

occurs; thus, the temperature at the time when the air parcel was last saturated dictates its water vapor content. Given the temperature at the point of last condensation (inferred from given wind and temperature fields) and the temperature at the desired target point, these models explain much of the observed variability in relative humidity in the free troposphere. However, near a land surface, this model breaks down, because the air parcel is subject to additional inputs of heat and moisture (surface sensible heating and surface evapotranspiration, respectively). As we will show, surface fluxes are strongly linked to RH, to the extent that an air parcel's back trajectory and saturation history are not essential to explaining variability in near-surface relative humidity. Thus, the advection-condensation model is an inappropriate tool for understanding near-surface relative humidity (Sherwood et al. 2010b). Another common model for relative humidity in the free troposphere is the bulk plume model (e.g., Romps 2014; Singh et al. 2019), which assumes that the atmosphere is composed of entraining plumes. This assumption does not hold near the surface either. Therefore, we need a different approach to understand near-surface relative humidity.

In this study, we derive an analytic relation between RH and surface fluxes over land, based on an idealized energy balance of the atmospheric column above and below the lifting condensation level (LCL). Similar approaches have been used over ocean to relate radiative cooling above the LCL to precipitation (Sarachik 1978, 1985; Betts and Ridgway 1989; Allen and Ingram 2002; Takahashi 2009; O'Gorman et al. 2012; Jeevanjee and Romps 2018) but, to our knowledge, have not been explored over land. The most relevant previous studies over land use conceptual models of the diurnally averaged atmospheric boundary layer (Betts 1994; Brubaker and Entekhabi 1995; Entekhabi and Brubaker 1995; Brubaker and Entekhabi 1996; Kim and Entekhabi 1998; Betts 2000). Our approach differs from these studies in several important respects. First, rather than making qualitative comparisons based on numerical simulations, we derive an analytic relation between RH and the evaporative fraction (EF), the fraction of surface energy used in evapotranspiration. The analytic relation has no calibrated parameters and is based on simple physics. Second, we evaluate the analytic relation using cloud-permitting simulations, which were not available

when the most relevant previous studies were conducted. Third, our conceptual model is simpler than those in previous studies. In particular, we make a purely energetic argument, whereas previous studies use more complicated models that include moisture budgets. We also simplify the problem by treating the atmospheric column as in radiative-convective equilibrium (RCE). Miyawaki et al. (2022) showed that an approximate form of RCE is a surprisingly reasonable model of the atmosphere over real-world land surfaces outside high latitudes, at least in the time and zonal means.

This article is structured as follows. In section 2, we derive the theory and discuss its assumptions and limitations. In section 3, the theory is tested using a suite of cloud-permitting simulations over idealized land surfaces. The theory is then used to answer the two sets of questions posed earlier (sections 4 and 5, respectively). The manuscript concludes with a summary and a brief discussion of potential future applications of the theory (section 6).

2. Theory

We first introduce a simple model to describe the basic physical mechanisms that comprise the theory. The intent of this model is to identify the most essential mechanisms governing RH over land. It is not intended as a replacement for GCMs or other more complex simulations.

The model is summarized in Fig. 2. At equilibrium, the surface sensible heat flux is balanced by diabatic cooling below the lifting condensation level (LCL), with heat convergence assumed negligible. Specifically, the enthalpy budget below the LCL is

$$H = \frac{c_p(p_s - p_{\text{LCL}})}{g} [Q_R(p_{\text{LCL}}) + Q_P(p_{\text{LCL}})], \quad (1)$$

where H is the surface sensible heat flux (W m^{-2}), c_p is the specific heat capacity of air at constant pressure ($\text{J kg}^{-1} \text{K}^{-1}$), g is gravitational acceleration (m s^{-2}), p_s and p_{LCL} are the pressures at the surface and LCL, respectively (Pa), and $Q_R(p_{\text{LCL}})$ and $Q_P(p_{\text{LCL}})$ are the cooling rates (K s^{-1}) averaged between the surface and LCL due to radiative cooling and precipitation re-evaporation, respectively. A derivation is provided in appendix A. Figure 3 shows schematically how the diabatic cooling rate Q (K s^{-1}) for a volume of air with thickness Δp (Pa) relates to its diabatic cooling flux density (W m^{-2}): for a given Q , the diabatic cooling flux density is larger when the volume of air is thicker (greater Δp). Thus, Eq. (1) says that a larger surface sensible heat flux must be balanced by either a deeper LCL or a greater diabatic cooling rate below the LCL, or both. Equation (1) is similar to Eq. (6) of Betts (2000), except we neglect the turbulent flux at the LCL. That assumption is justified because, as shown in Driedonks (1982), a large majority of the energy that is turbulently entrained into the boundary layer from the free troposphere is used to grow the boundary layer, rather than warm it. Broadly similar conceptual models are also used in Betts and Ridgway (1989) and Takahashi (2009) over ocean, and it is complementary to the common energetic argument that radiative cooling balances diabatic heating from condensation

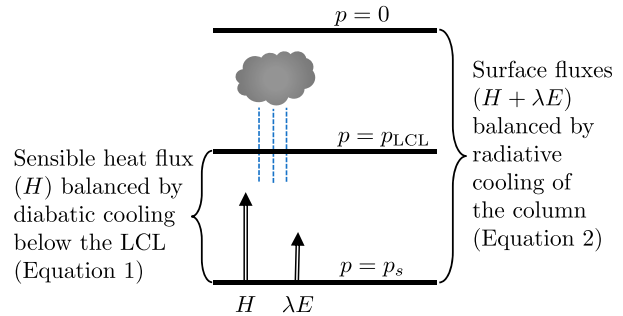


FIG. 2. Schematic of the simple model from which the theory is derived. The sum of surface sensible and latent heat fluxes (H and λE , respectively) is balanced by the radiative cooling of the column. The sensible heat flux is balanced by diabatic cooling (both radiative cooling and re-evaporation of falling hydrometeors) below the lifting condensation level (LCL; corresponding to the pressure level of p_{LCL}). The theory's main predictions are Eqs. (5) and (6). The atmospheric pressure p is p_s at the surface, and zero at the top of the atmosphere.

above the LCL (Betts and Ridgway 1989; Allen and Ingram 2002; Takahashi 2009; O'Gorman et al. 2012; Jeevanjee and Romps 2018; note that these studies neglect the precipitation re-evaporation term).

Next, the atmosphere is assumed to be in a state of radiative-convective equilibrium (RCE), in which the surface flux of moist static energy (equivalent to the sum of the surface latent heat flux and sensible heat flux) exactly balances the net radiative cooling of the atmospheric column, with negligible net advection of moist static energy (Neelin and Held 1987; Beucler and Cronin 2016):

$$\lambda E + H = \frac{c_p p_s}{g} Q_R(0), \quad (2)$$

where λ is the latent heat of vaporization of water (J kg^{-1}), λE is the surface latent heat flux due to evaporation (W m^{-2}), and $Q_R(0)$ is the radiative cooling rate (K s^{-1}) averaged between the surface and the top of the atmosphere ($p = 0$). Note that, unlike Eq. (1), diabatic heating/cooling from condensation/precipitation re-evaporation is not present in the moist static energy budget due to terms cancelling in its derivation [see Eqs. (2.2)–(2.4) of Neelin and Held (1987)]. Clearly, RCE is an idealized state that is only strictly true in the global mean, and is often used as a reasonable simplification of the tropics. However, Miyawaki et al. (2022) found that its utility as a simple approximation of the zonally and temporally averaged climate extends well beyond the tropics: they also find an approximate RCE state extends as far as 40°N . The major cause is the presence of land: aquaplanet simulations with a small heat capacity surface (an idealization of a land surface) produced midlatitudes that were in approximate RCE during summer, whereas simulations with a large heat capacity did not. We will examine the sensitivity of the theory's predictions to the RCE assumption in the next section.

The evaporative fraction (EF) is the ratio of the surface latent heat flux to the available energy at the surface (the

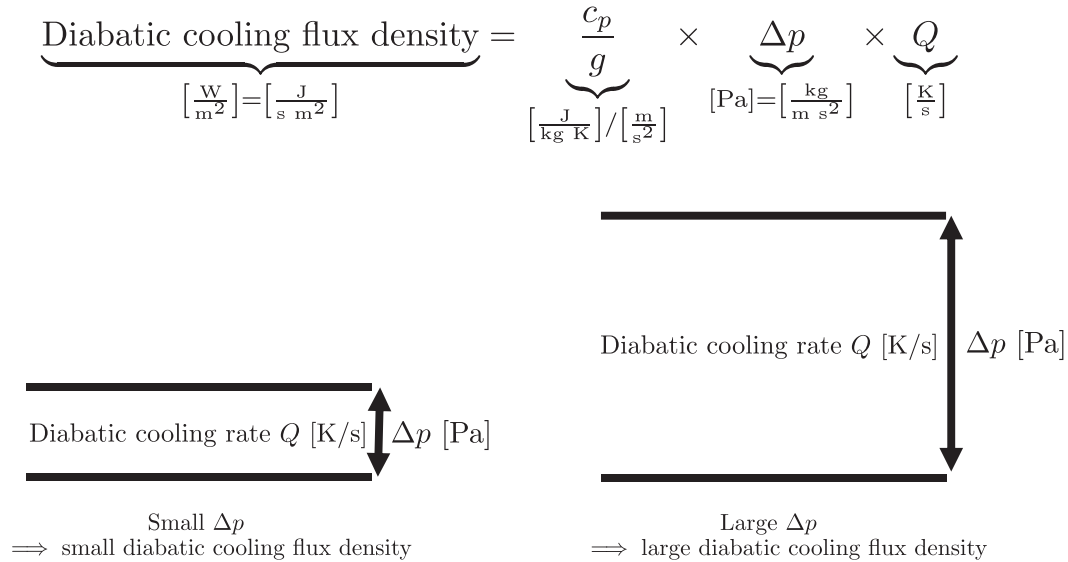


FIG. 3. Relation between the diabatic cooling rate Q (K s^{-1}) for a volume of air with thickness Δp (Pa) and its diabatic cooling flux density (W m^{-2}).

sum of the surface latent and sensible heat fluxes). Combining Eqs. (1) and (2) yields

$$\text{EF} = 1 - \underbrace{\frac{Q_R(p_{\text{LCL}}) + Q_P(p_{\text{LCL}})}{Q_R(0)}}_{=\beta} \left(1 - \frac{p_{\text{LCL}}}{p_s}\right). \quad (3)$$

Since β is a function of precipitation re-evaporation, which is subject to considerable uncertainty, we do not attempt to provide a simple physical model of β . Instead, we will use cloud-permitting simulations to show that β can be approximated as a constant under a wide range of conditions, at least to first order (section 3). This implies that EF and p_{LCL}/p_s are linearly related. Betts (1994) recognized fundamental links between RH, EF, and p_{LCL} , and Betts (2000) noted that EF and p_{LCL} are linearly related based on numerical simulations, but neither study provided an analytic expression for the relation. Note that β is a function of observable atmospheric quantities and is not a calibrated parameter.

Finally, an exact expression for the height of the LCL—first derived in Yin et al. (2015) and also presented in Romps

(2017)—can be combined with this equation to directly relate EF and RH. The derivation provided in appendix B yields the relation

$$\text{EF} = 1 + \alpha \beta \log(\text{RH}), \quad (4)$$

where α is defined in Eq. (B3). Equivalently,

$$\text{RH} = \exp[-(\alpha\beta)^{-1}(1 - \text{EF})]. \quad (5)$$

Note that α is not a calibrated parameter, but a function of thermodynamic constants with weak dependence on temperature [specifically, the reference temperature T_0 , defined in Table 1; see Eq. (B3)]. It is essentially constant under typical conditions on Earth, varying between 0.21 at $T_0 = 270$ K and 0.26 at $T_0 = 310$ K. Using zonal mean near-surface air temperatures from the ERA5 reanalysis over both land and ocean, its range of variability is even smaller (Fig. 4b). Thus, $\alpha \approx 1/4$ is a reasonable approximation. In the next section, we will use cloud-permitting simulations to show that $\beta \approx 4$ across a wide range of conditions. While β cannot be directly estimated from the ERA5 reanalysis, its implied value can be

TABLE 1. Constants used in the derivation of Eq. (13), following the notation and values given in Romps (2017).

Variable	Definition	Value
E_{0v}	Difference in specific internal energy between water vapor and liquid at the triple point (J kg^{-1})	2.3740×10^6
c_{vv}	Specific heat capacity of water vapor at constant volume ($\text{J kg}^{-1} \text{K}^{-1}$)	1418
c_{vl}	Specific heat capacity of liquid water ($\text{J kg}^{-1} \text{K}^{-1}$)	4119
c_{va}	Specific heat capacity of dry air at constant volume ($\text{J kg}^{-1} \text{K}^{-1}$)	719
R_a	Specific gas constant of dry air ($\text{J kg}^{-1} \text{K}^{-1}$)	287.04
R_v	Specific gas constant of water vapor ($\text{J kg}^{-1} \text{K}^{-1}$)	461
$c_{pa} = c_{va} + R_a$	Specific heat capacity of dry air at constant pressure ($\text{J kg}^{-1} \text{K}^{-1}$)	—
$c_{pv} = c_{vv} + R_v$	Specific heat capacity of water vapor at constant pressure ($\text{J kg}^{-1} \text{K}^{-1}$)	—
T_{trip}	Triple-point temperature (K)	273.16
T_0	Reference temperature (K)	290

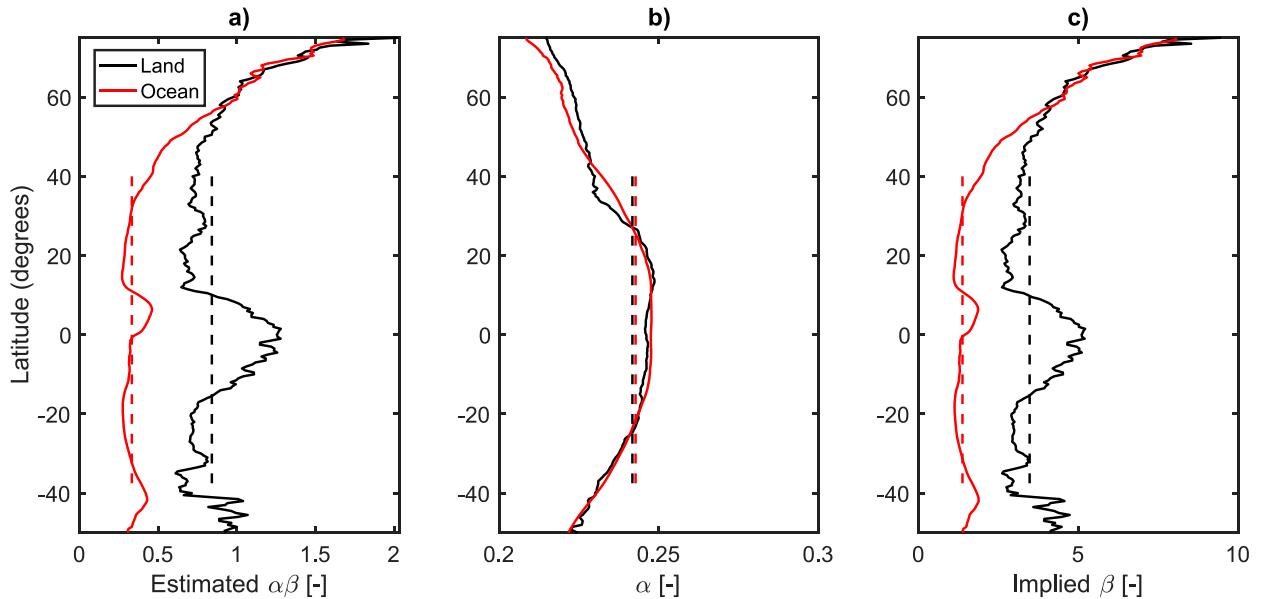


FIG. 4. Estimates of zonally averaged α and implied β obtained from the ERA5 reanalysis over land and ocean. In estimating α , the reanalysis near-surface air temperature is used as the reference temperature T_0 [Eq. (B3)]. Dashed lines show averages between 40°N and 40°S. Outside this region, the theory is not expected to hold.

estimated by combining Eq. (5) with reanalysis estimates of RH, EF, and α [qualitatively similar estimates are obtained using Eq. (B2) instead]. Zonal mean estimates of implied β over land in the ERA5 reanalysis agree reasonably with the $\beta \approx 4$ estimate obtained from cloud-permitting simulations (Fig. 4c). Combining the two approximations implies that $\alpha\beta \approx 1$, which is broadly supported by the reanalysis estimates over land (Fig. 4a). Thus, Eq. (5) can be further simplified to

$$\text{RH} \approx \exp[-(1 - \text{EF})]. \quad (6)$$

Equations (5) and (6) are the main predictions of the theory, with Eq. (6) being the simplest version of the theory. The predicted relation between RH and EF is shown in Fig. 5, along with its sensitivity to α and β . For the case in which $\beta = 4$, the exact relation [Eq. (B2)] is approximated reasonably by Eqs. (5) and (6), particularly for $\text{RH} > 0.5$ (Fig. 5a). The relation is relatively insensitive to the choice of α (Fig. 5c). It is more sensitive to β (Fig. 5b), and most sensitive when EF is low. As we will show, β varies within a fairly narrow range in cloud-permitting simulations, presented in the next section, with the values of β chosen in Fig. 5 reasonably representing that range.

Equation (6) reproduces RH in the ERA5 reanalysis quite well, outside high latitudes (Fig. 1c). Neither α nor β is tuned to the reanalysis. Rather, the characteristic values used in the theory are chosen to maximize the theory's simplicity, within the tight constraints imposed by Eq. (B3) (for α) and the cloud-permitting simulations presented in the next section (for β). Still, it is important to consider the degree to which the fit may be simply a fortuitous result of compensating errors. Figure 6a shows the sensitivity of the profile to approximations made in deriving Eq. (6) from Eq. (B2). The simplest

version of the theory [Eq. (6)] slightly overestimates RH relative to Eq. (5) and the exact relation [Eq. (B2)] in the dry subtropics. This results in the simplest version of the theory fitting the reanalysis slightly better than it should in the Northern Hemisphere ($\sim 20^\circ\text{N}$), and slightly worse than it should in the Southern Hemisphere ($\sim 20^\circ\text{S}$). Figure 6b shows that the fit is more sensitive to the choice of β . However, even choosing a value at the bottom of the range observed in simulations ($\beta \approx 3$) still results in a W-shaped RH profile, with values consistently well above 1%, meaning the theory still reproduces the main features we seek to explain. Finally, Fig. 6c shows that the fit is very insensitive to varying T_0 (and, thus, α). Overall, the fit is not particularly sensitive to reasonable deviations from the approximations made in deriving Eq. (6).

As noted earlier, the values of β estimated directly from the cloud-permitting simulations (Fig. 7d) are qualitatively similar to those estimated indirectly from the reanalysis (Fig. 4c). There is some spatial structure to deviations of β from the value of $\beta = 4$ used in the theory. Some of that structure is explained by deviations from RCE: for example, as discussed later in the manuscript, at high latitudes Eq. (8) predicts that β should grow rapidly, as observed, since R_1 approaches one. Other aspects of the structure are not explained by deviations from RCE: in particular, Eq. (8) predicts that, if anything, β should be lower in the tropics than in the subtropics [since R_1 is most negative in the tropics in Fig. 4 of Miyawaki et al. (2022)]. Outside high latitudes, the implied values of β deviate most from $\beta = 4$ near the equator. It is unclear how meaningful these deviations are, given the limitations in precipitation re-evaporation and radiative cooling in the reanalysis noted above. Also, the theory's RH predictions

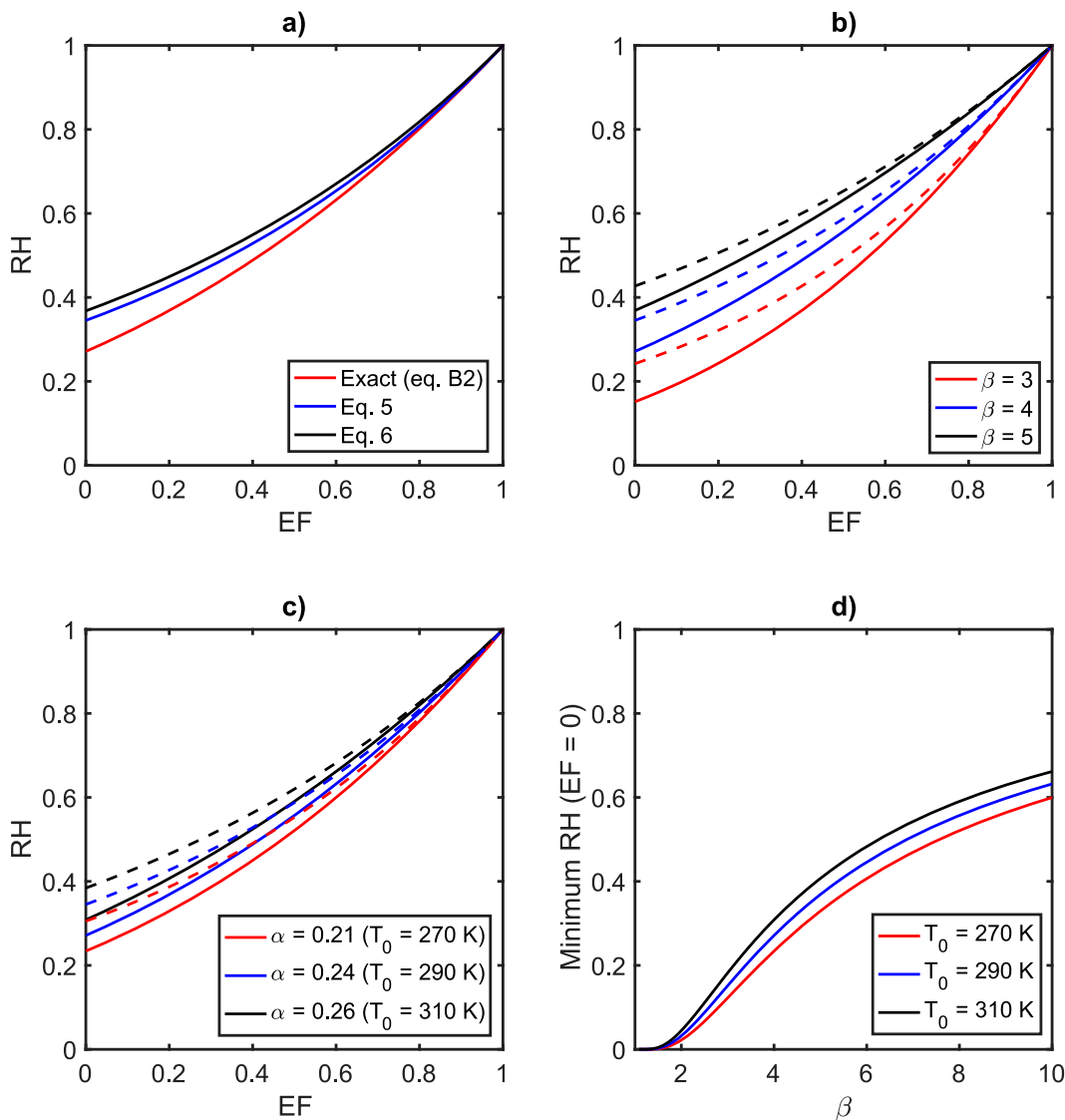


FIG. 5. The theory's predicted relation between RH and EF. Unless otherwise marked, default values used are $\beta = 4$ and $T_0 = 290$ K. (a) Comparison between the exact relation [Eq. (B2)], and two approximations [Eq. (5), with α estimated using Eq. (B3), and Eq. (6)]. (b) Sensitivity of the relation to varying β , for both the exact relation [Eq. (B2), solid lines] and the approximation in Eq. (5) (dashed lines). (c) As in (b), but for sensitivity to varying α [which is a function of T_0 ; Eq. (B3)]. (d) Sensitivity of the minimum RH (corresponding to $EF = 0$) to β and T_0 , using the exact relation [Eq. (B2)].

are least sensitive to β in regions with high EF (Fig. 5b), such as those near the equator.

How does the theory perform in extreme limiting cases? Over a perfectly dry land surface in RCE, there is no water vapor, no precipitation, and both EF and RH must be exactly zero. The LCL extends to the top of the column [$Q_R(p_{LCL}) = Q_R(0)$], there is no precipitation re-evaporation [$Q_P(p_{LCL}) = 0$], and thus $\beta = 1$. The exact theory correctly diagnoses RH as exactly zero in this case [Eq. (B2)], but not the simpler approximations [Eqs. (5) and (6)]. Over a saturated land surface, both EF and RH approach 1 as air temperatures rise (Raupach 2001). All versions of the theory

correctly diagnose RH in this limiting case, for any finite and positive β .

a. Interpretation

The theory links RH and EF but does not make claims about the causal relation between RH and EF. Does variability in RH cause variability in EF, or vice versa? Or does an entirely separate mechanism cause coincident variability in both RH and EF? All three options are likely true, to some extent, but variability in EF is certainly *sufficient* to cause variability in RH on its own. There is substantial modeling

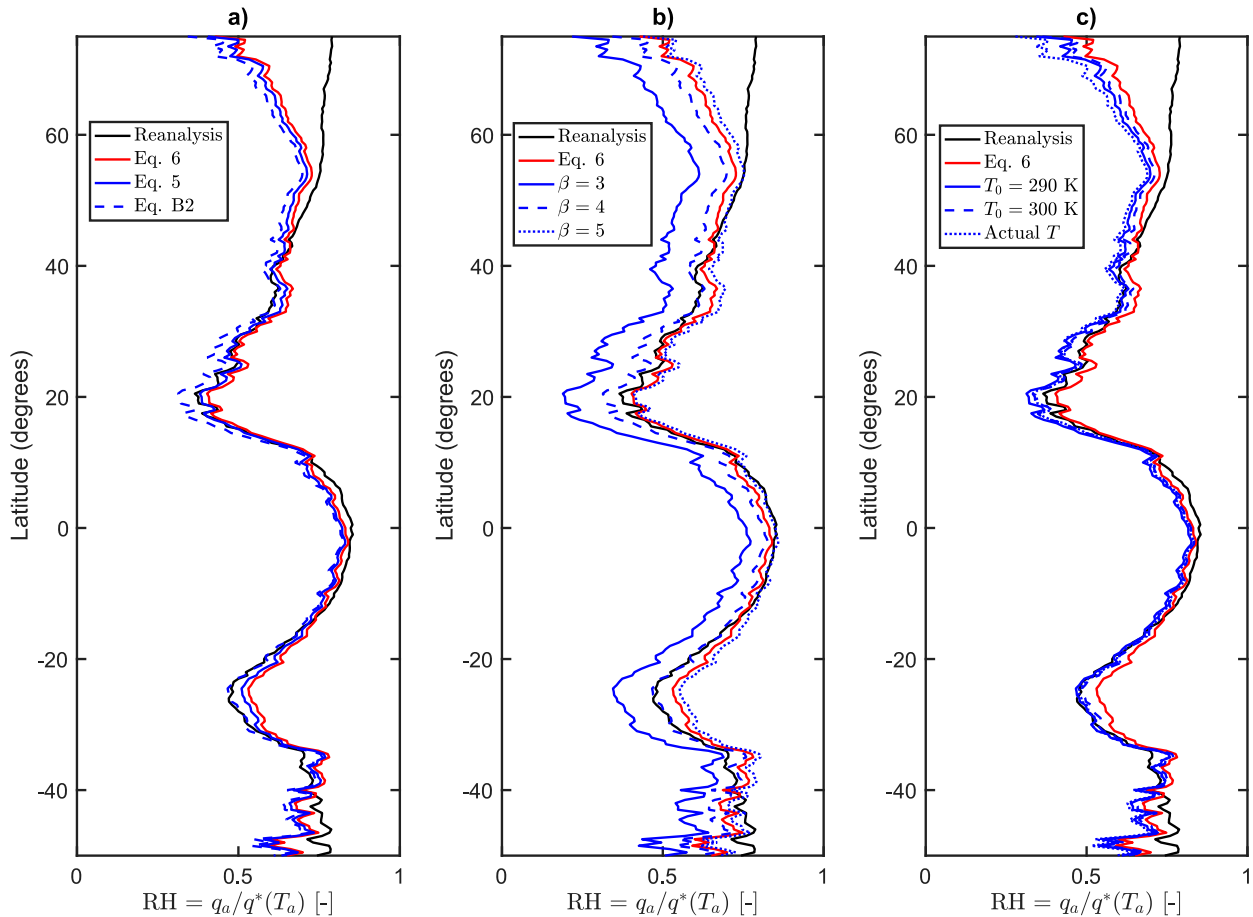


FIG. 6. Sensitivity of the land zonally averaged RH profile to approximations made in the theory. The solid red and black lines are identical to those in Fig. 1d. Unless otherwise marked, the exact relation [Eq. (B2)] is used with $\beta = 4$ and $T_0 = 290$ K. (a) Comparison between the exact relation [Eq. (B2)] and two approximations [Eq. (5) with α estimated using Eq. (B3), and Eq. (6)]. (b) Sensitivity of the relation to varying β . (c) As in (b), but for sensitivity to varying α (which is a function of T_0). “Actual T ” refers to setting T_0 equal to the zonally varying near-surface air temperature obtained from the reanalysis.

evidence that variability in soil moisture—which is the first-order control on EF in the current climate (Koster et al. 2009; Seneviratne et al. 2010; Koster and Mahanama 2012)—is capable of causing variability in RH. In even the earliest climate models, mechanism-denial experiments showed that persistent anomalies in soil moisture cause persistent anomalies in RH (Delworth and Manabe 1989). Reductions in global mean soil moisture cause reductions in global mean RH in modern models of Earth (Krakauer et al. 2010; Laguë et al. 2023) and idealized land planets (Becker and Stevens 2014; they modify surface resistance, rather than soil moisture, but it is functionally similar). Simulations of idealized land planets with prescribed soil water concentrated at the poles result in consistently low RH throughout the tropics and subtropics (Kodama et al. 2018). And, in climate change simulations, the combined effects of declining soil moisture and increasing plant water-use efficiency largely cause reductions in RH (Berg et al. 2016; Zhou et al. 2023). In section 3, we will show that cloud-permitting simulations with fixed soil moisture in RCE reproduce the theory very well, implying that

soil moisture variability causes variability in RH in the simulations.

While there is abundant evidence that variability in soil moisture and EF is *sufficient* to cause variability in RH, we do not claim that it is *necessary*. Other atmospheric mechanisms may exist that are unrelated to the mechanism proposed here. It is well known that atmospheric mechanisms are sufficient to produce a W-shaped profile in free tropospheric relative humidity in aquaplanet simulations (Frierson et al. 2006; O’Gorman and Schneider 2008; O’Gorman et al. 2011). On the other hand, while the W-shaped profile in relative humidity is prominent in the free troposphere, it is barely visible in the near-surface atmosphere in the same aquaplanet simulations [see, e.g., Fig. 6 of Frierson et al. (2006), Fig. 1 of O’Gorman and Schneider (2008), or Fig. 9 of O’Gorman et al. (2011)].

b. Limitations

The theory’s most significant limitation is its neglect of advection and convergence from outside the atmospheric column. Obviously, advection exists and is almost never strictly

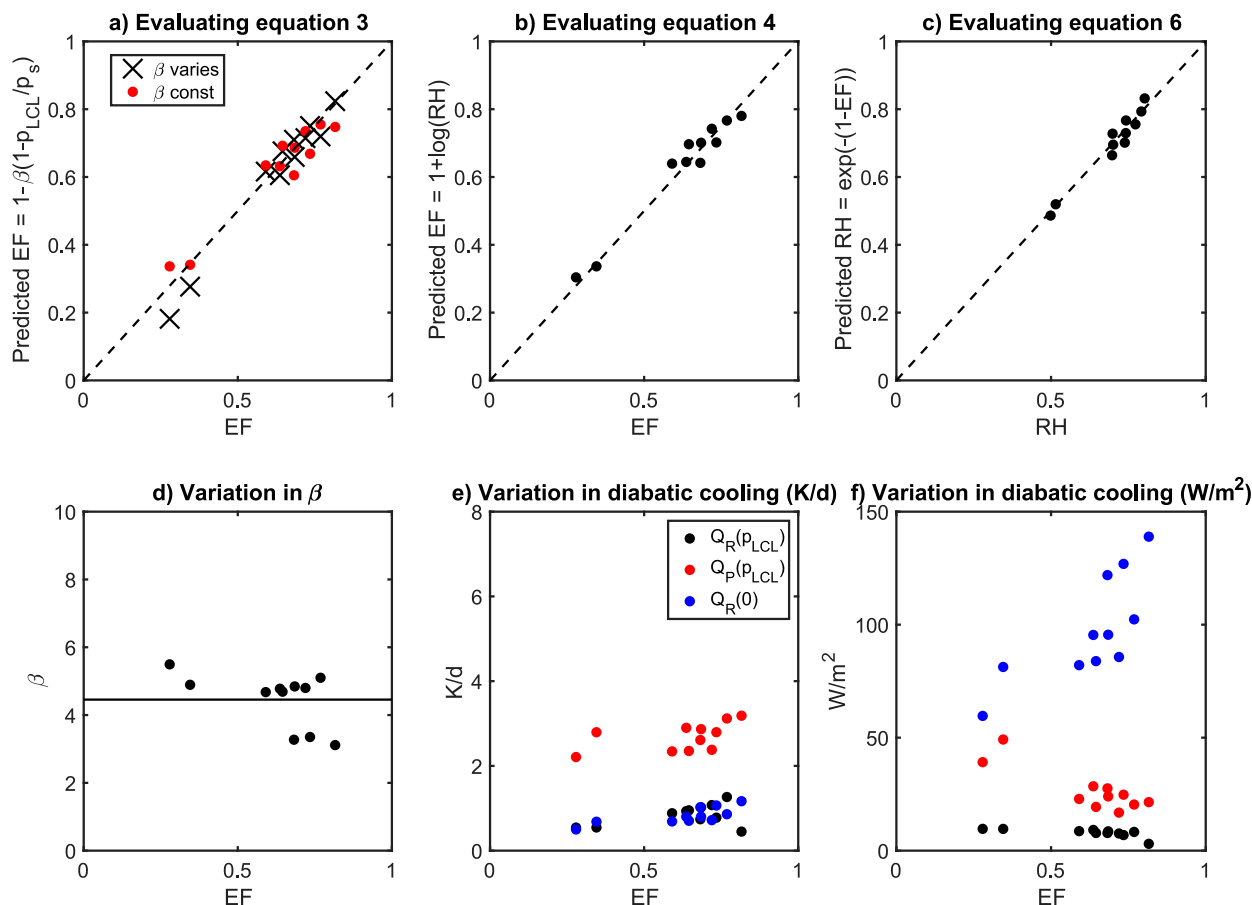


FIG. 7. Evaluating the theory using cloud permitting simulations over an idealized land surface. (a) Comparison between simulated EF and predicted EF [Eq. (3)]. Each dot is a separate simulation. Black crosses show results in which β was estimated individually for each simulation. Red dots show results in which the average value of β across all simulations was used in testing the predicted EF for each simulation. (b) Comparison between simulated EF and predicted EF [Eq. (4) with $\alpha\beta = 1$]. (c) Comparison between simulated RH and predicted RH [Eq. (6)]. (d) Variability of β between simulations, with different values of EF. The black line is the average value across simulations. (e) Variability of the radiative cooling rate below the LCL [$Q_R(p_{\text{LCL}})$; black dots], precipitation re-evaporation cooling rate below the LCL [$Q_P(p_{\text{LCL}})$; red dots], and radiative cooling rate of the entire atmospheric column [$Q_R(0)$; blue dots] between simulations, with different values of EF. (f) As in (e), but showing cooling flux densities, rather than cooling rates.

zero. The relevant questions are these: Is advection comparable to or larger than the other terms in Eqs. (1) and (2)? And how sensitive is the theory to the assumption of zero advection? Over zonally averaged land surfaces outside high latitudes, we argue that advection is typically small relative to other terms in the budgets above, and the theory's main conclusions are qualitatively insensitive to its neglect.

We illustrate this point by relaxing the assumption of RCE in Eq. (2). The equation is rewritten to include the neglected storage term and meridional divergence terms in the column-averaged moist static energy budget. Using the same notation as Miyawaki et al. (2022), it is

$$\lambda E + H = (1 - R_1) \frac{c_p p_s}{g} Q_R(0), \quad (7)$$

where R_1 is the ratio of the sum of the storage and meridional divergence terms to the radiative cooling term. Continuing

with the derivation as above, the only effect of relaxing the RCE assumption is to alter the definition of β to be

$$\beta' = \frac{Q_R(p_{\text{LCL}}) + Q_P(p_{\text{LCL}})}{(1 - R_1)Q_R(0)} = \frac{\beta}{1 - R_1}, \quad (8)$$

where β' is distinguished from β , defined earlier. As shown in Fig. 2 of Miyawaki et al. (2022), R_1 varies between -0.4 and 0.1 from the equator to latitudes of $\pm 40^\circ$, based on their analysis of the ERA5 reanalysis. Therefore, in this region, deviations from the RCE assumption would result in β being multiplied by a factor somewhere between 0.7 and 1.1 . This is arguably comparable to the uncertainty in β caused by uncertainties in parameterizations of precipitation re-evaporation or near-surface radiative fluxes. In any case, it does not change the sign of β or its order of magnitude. Thus, the main results of the theory are relatively insensitive to the RCE assumption, at least between the equator and latitudes of $\pm 40^\circ$.

We do not claim that the theory holds at higher latitudes: in fact, the theory should not work in these regions, because the assumption of RCE is badly violated. Indeed, since R_1 approaches 1 at higher latitudes, Eq. (8) predicts that the value of β' implied by the reanalysis should grow rapidly. This is exactly what is seen in Fig. 4c.

Another possible criticism of this theory is that it is not fundamental. Like other theories of RH in the free troposphere (e.g., Sherwood 1996; Romps 2014; Singh et al. 2019), our theory is diagnostic: specifically, it relates RH and EF. Of course, EF is itself controlled by other variables, particularly precipitation. Could the theory be simpler, perhaps by relating EF to precipitation or some other quantity? We will explore this further in section 5. It is certainly true that much of the observed zonal-mean spatial variability in EF in the current climate can be explained by variability in precipitation. However, there is important variability in EF that is not explained by variability in precipitation, particularly in a warming world. Earth system models show that RH declines over land, on average, as CO_2 concentrations increase even when the radiative effects of CO_2 are eliminated entirely (Cao et al. 2010; Andrews et al. 2011; Swann et al. 2016; Berg et al. 2016). This is due to the plant physiological response, in which plants transpire less, all else being equal, when CO_2 concentrations are greater, and is entirely separate from changes in precipitation caused by greenhouse warming. For these reasons, any theory of future changes in RH must be tightly linked to surface evaporation. Even theories linking changes in RH over land to changes in ocean variables (Byrne and O’Gorman 2016, 2018) ultimately still acknowledge the central importance of evapotranspiration. More broadly, any truly definitive theory should be able to explain variability in RH caused by human modifications to the landscape, such as those due to large-scale irrigation or land-use change.

3. Evaluating the theory with cloud-permitting simulations

To evaluate the theory, we conducted cloud-permitting simulations over an idealized land surface in RCE. Specifically, we conducted simulations using the System for Atmospheric Modeling (SAM; Khairoutdinov and Randall 2003) version 6.11.1, using the Community Atmosphere Model version 3 (CAM3) radiative transfer scheme, a single-moment microphysics scheme, and a 1.5-order turbulent kinetic energy (TKE) subgrid-scale turbulence closure scheme. The Simplified Land Model (SLM; Lee and Khairoutdinov 2015) was used with a homogeneous grassland surface to simulate the lower boundary. In simulations over ocean, it is common to use prescribed sea surface temperatures as the lower boundary condition. Over land, this boundary condition is inappropriate: land has a much lower heat capacity, meaning surface temperature responds rapidly to changes in radiative forcing and water limitation, and is thus an interactive state variable rather than a fixed boundary condition. Instead of fixing surface temperature, we fix daily mean surface soil moisture, which varies on longer time scales than surface temperature, and is thus the more appropriate boundary condition. This is

analogous to a situation in which surface moisture is largely controlled by factors other than rainfall, such as irrigation using water pumped from groundwater aquifers. Instead of fixing soil moisture, we could have fixed neither soil moisture nor temperature and instead simply used the surface energy budget as the lower boundary condition. We did not do this because the resulting simulations span a relatively narrow range of soil moisture values (not shown). We also aim to show that variability in soil moisture and EF is sufficient to cause variability in RH, and fixing soil moisture allows us to identify the direction of causality.

Twelve simulations were conducted, using three different values for solar forcing (equivalent to solar forcing at latitudes of 8° , 12° , and 16°N) and four different values of soil saturation [0.2, 0.4, 0.6, and 1.0 (dimensionless)]. Rather than exactly fixing soil moisture to the assigned value, the soil moisture states were relaxed to the assigned value on a relaxation time scale of 24 h. We simulated a square domain with a width of 192 km, a horizontal spatial resolution of 3 km, and doubly periodic lateral boundary conditions. In the 64 vertical model levels, 12 levels are in the lowest 1 km, and 34 levels are in the lowest 10 km, with the upper boundary at 26 km. Each simulation was run for 1000 days to reach a radiative–convective quasi-equilibrium state, with the last 30 days of the simulation used to estimate averages. The case at latitude 8°N and soil saturation of 1.0 did not converge, and was eliminated from subsequent analyses.

Figure 7 compares the theory’s predictions to those from the cloud-permitting simulations. The theory reproduces Eqs. (3) (Fig. 7a), (4) (Fig. 7b), and (6) (Fig. 7c) quite well across a broad range of simulated conditions. Similar results are obtained from simulations with interactive soil moisture, although they span a narrower range of EF and RH (not shown).

There is relatively little variation in β between simulations (Fig. 7d). The estimated mean value is close to $\beta = 4$, justifying the approximation $\alpha\beta \approx 1$. Using the mean value of β across simulations (Fig. 7a, red dots), rather than an interactively varying β (Fig. 7a, black crosses), does not substantially degrade the theory’s performance.

The three diabatic cooling terms that determine β are shown in terms of cooling rates (K day^{-1} ; Fig. 7e) and cooling flux densities (W m^{-2} ; Fig. 7f). The total column radiative cooling flux density (the difference between OLR and net surface longwave radiation) increases significantly with increasing EF (Fig. 7f, blue dots) and is greater than both radiative and precipitation re-evaporation cooling flux densities below the LCL (black and red dots, respectively). However, when converted to cooling rates, the precipitation re-evaporation cooling rate below the LCL (Fig. 7e, red dots) exceeds the radiative cooling rates of both the total atmospheric column (blue dots) and the atmosphere below the LCL (black dots). The reason for this difference is that the pressure thickness of the total column is greater than that of the atmosphere below the LCL. Thus, the blue dots in Fig. 7f are divided by a larger number (the pressure thickness of the entire column) to obtain cooling rates in Fig. 7e, compared to the red dots (which are divided by the pressure thickness of the atmosphere below the LCL).

Values of β that are an order of magnitude smaller or larger would not be internally consistent with our theory, at least for conditions typical of the modern Earth. The radiative cooling rate below the LCL [$Q_R(p_{LCL})$] is similar to that of the entire column [$Q_R(0)$] in our simulations (Fig. 7e). Since $Q_R(p_{LCL}) \geq 0$ (because no condensational heating occurs below the LCL, by definition), the first-order approximation $Q_R(p_{LCL}) \approx Q_R(0)$ directly implies that $\beta \geq 1$, meaning β could not be an order of magnitude smaller. Over land and outside high latitudes, the zonally and temporally averaged EF is always nonnegative, which provides an upper bound on β . Figure 5d shows the upper bound on β (horizontal axis) for a given RH (vertical axis), calculated using Eq. (B2). The upper bound on β increases with increasing RH, and diverges to infinity as RH approaches one. Physically, exceeding this upper bound corresponds to precipitation re-evaporation below the LCL exceeding the net condensation rate above the LCL, requiring condensation at the land surface (negative λE) to balance the atmospheric water budget. If β was an order of magnitude larger ($\beta \approx 40$), this bound would require $RH \gtrsim 0.9$. Such values of RH do not arise anywhere over land, at least in the zonal and temporal average for the modern Earth (Fig. 1c), precluding β from being an order of magnitude larger.

Since the diabatic cooling terms are all partially functions of RH, it might seem better to write equations for these terms that make that dependence explicit, and include it in the theory. We did not do this for two reasons. First, the dependence of precipitation re-evaporation on RH is, at best, semiempirical. For example, a recently proposed scaling relation linking precipitation re-evaporation and RH (Lutsko and Cronin 2018) would introduce at least one calibration parameter. Second, the near-surface radiative cooling in the cloud-permitting simulations is likely subject to considerable numerical errors due to the coarse grid resolution near the surface [see, e.g., Fig. 10 of Ha and Mahrt (2003)]. Given these uncertainties, it seems prudent to avoid overfitting our theory.

4. Explaining the observed range of variability of RH

Using the theory derived in the previous section, we can answer the first set of questions posed in the introduction. Recall that we refer to “RH” as shorthand for “zonally and temporally averaged near-surface RH.”

a. Lower bound over land

First, why is RH never extremely low (e.g., 1%) over land? Outside high latitudes, EF is always nonnegative over land, at least for zonal and temporal averages. Therefore, all else being equal, the theory predicts that RH will be lowest when EF is zero. Figure 5d shows the theory’s predicted RH when EF is zero, using Eq. (B2). Note that we do not use the simpler version of the theory [Eq. (5)] for this analysis because it is least accurate for especially low values of EF. The predicted lower bound on RH is only weakly sensitive to temperature, but is more sensitive to β . For the characteristic value of $\beta = 4$ consistent with our cloud-permitting simulations, the predicted lower bound on RH is $\sim 20\%$. The lower bound on RH increases further with increasing β . Thus, the theory precludes

extremely low values of RH over land, given typical values of β and temperature.

What conditions would permit especially low values of RH? Figure 5d shows that especially low values of β permit especially low RH. Specifically, the lower bound on RH is zero for $\beta = 1$, and remains close to it for $\beta \lesssim 2$. Those conditions do not appear typical of the modern Earth. We do not observe $\beta \leq 2$ in any of our cloud-permitting simulations (Fig. 7d), nor in values inferred from the reanalysis over land (Fig. 4c). But some humility is warranted. Recall that β is a function of radiative and (precipitation re)evaporative cooling. Precipitation re-evaporation is highly parameterized in models. Both precipitation re-evaporation (Jeevanjee and Zhou 2022) and near-surface radiative cooling (Ha and Mahrt 2003) are sensitive to model resolution. Observations of both quantities are limited.

On the other hand, both theory and available observations suggest that $\beta \lesssim 2$ is unlikely, at least for conditions typical of the modern Earth. Any reasonable amount of precipitation re-evaporation below the LCL will likely increase β above such a threshold. And, while precipitation re-evaporation is dependent on model resolution, it tends to increase with increasing resolution [see Fig. 2 of Jeevanjee and Zhou (2022)]. That suggests that, if anything, models typically underestimate it, and therefore typically underestimate β . Even in the absence of precipitation re-evaporation below the LCL, there is still some reason to expect that radiative cooling near the surface will be larger than its column average, which could also lead to β exceeding the threshold. Pierrehumbert (2010) considers a gray gas atmosphere with a dry adiabatic temperature profile (his section 4.3.2). His Fig. 4.2 shows that, even in this idealized case, radiative cooling (corresponding to increasing net infrared flux with height) is greatest near the surface. Qualitatively similar results are seen in Figs. 6 and 7 of Jeevanjee and Fueglistaler (2020), who perform line-by-line radiative transfer calculations. Observations of radiative cooling rates in the lowest few meters of the atmosphere are rare. However, one site in the Netherlands shows values on the order of -10 to -20 K day^{-1} during the summer, substantially stronger (more negative) than those generally obtained from numerical simulations (Gentine et al. 2018). Also, recent observations of clear-sky radiative cooling profiles in the tropical Atlantic show large peaks near the top of the boundary layer, caused by sharp gradients in humidity (Fildier et al. 2023). While those observations are taken over ocean, the same mechanism could conceivably extend to land.

In summary, the theory provides a lower bound on RH that is a function of β . For typical values of β diagnosed from cloud-permitting simulations, it predicts a lower bound of $\sim 20\%$. For $\beta \lesssim 2$, especially low values of RH are permitted. However, for various reasons, such conditions appear unlikely to occur in the current climate. Definitively ruling out the possibility would require advances in understanding of radiative cooling and precipitation re-evaporation over land.

b. Lower bound over a saturated surface

A tighter lower bound on RH is possible for a saturated surface in RCE, such as an ocean. Philip (1987) derived an

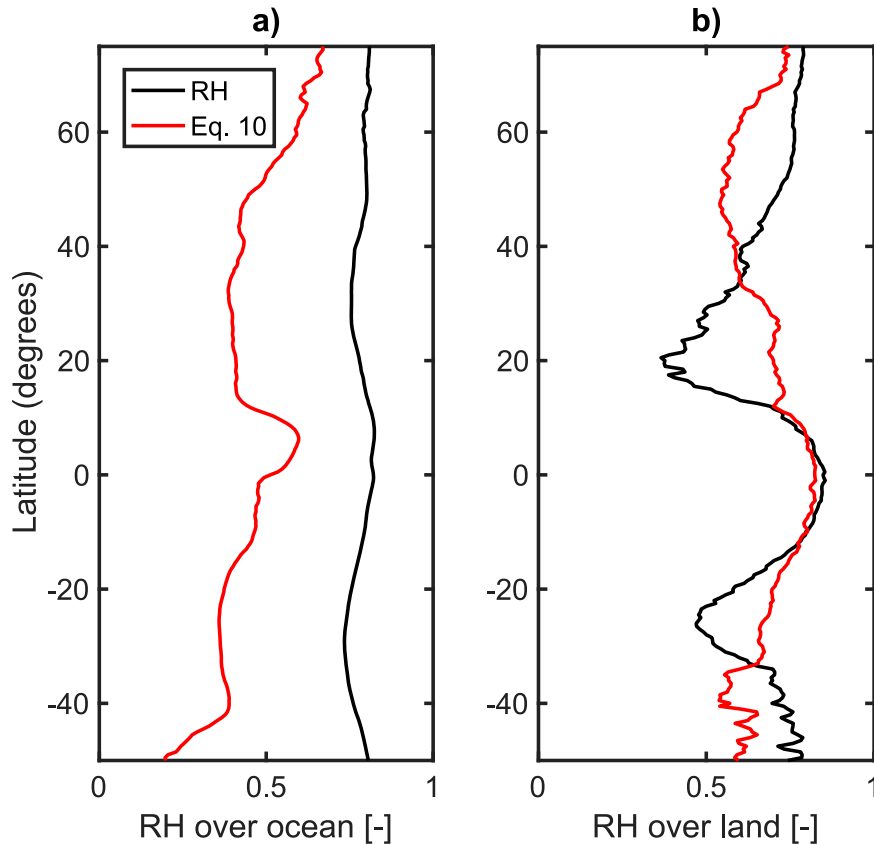


FIG. 8. RH and predicted lower bound on RH over a saturated surface [Eq. (10)], estimated over (a) ocean and (b) land. Values of α and β are estimated from the ERA5 reanalysis, as in Fig. 4. Note that most land is not saturated, meaning the actual RH is often lower than the predicted lower bound on RH for a saturated surface.

upper bound on the Bowen ratio over a saturated surface that arises by forbidding supersaturation. This bound is equivalent to a lower bound on EF:

$$EF \geq EF_{eq} = \frac{\lambda^2 q^*(T_a)}{\lambda^2 q^*(T_a) + R_v c_p T_a^2} \quad (9)$$

where EF_{eq} is the evaporative fraction corresponding to “equilibrium evaporation” (Slatyer and McIlroy 1961; Priestley and Taylor 1972; McNaughton 1976a,b; Raupach 2001). The physical arguments presented by Philip (1987) in support of this bound are reviewed in appendix C. In the ERA5 reanalysis, averaging over land between 40°N and 40°S gives a value of $EF_{eq} = 0.72$. This lower bound on EF is similar to actual values of EF over saturated land surfaces in climate models (Koster and Mahanama 2012; Milly and Dunne 2016) and observations (Maes et al. 2019), and thus appears to provide a relatively tight constraint on the actual EF over saturated surfaces.

Combining the lower bound for EF with our theory then implies the following bound for RH over a saturated surface in RCE:

$$RH \geq \exp[-(\alpha\beta)^{-1}(1 - EF_{eq})] = \exp\left[-(\alpha\beta)^{-1} \frac{R_v c_p T_a^2}{\lambda^2 q^*(T_a) + R_v c_p T_a^2}\right]. \quad (10)$$

The lower bound is plotted in Fig. 8 using reanalysis data and compared with the reanalysis RH over ocean (Fig. 8a) and land (Fig. 8b). The lower bound is nontrivial: near the equator, it approaches 60% over ocean, and exceeds 80% over land. Land is generally not saturated, particularly in the zonal mean, so the lower bound for a saturated surface often exceeds the actual RH.

An important caveat, for both the lower bounds over ocean and land, is that the lower bound only holds to the extent that Eqs. (1) and (2) are satisfied. Substantial moisture convergence, for example, would be inconsistent with these equations, and could plausibly play a role in setting a lower bound on RH, particularly over land. On balance, these equations appear to reasonably approximate the dominant mechanisms over land, in which dry soils create a large surface sensible heat flux. Over ocean, however, the sensible heat flux is much less pronounced because the surface is always saturated. It is

also not clear that RCE remains a reasonable approximation away from the equator over ocean. On the other hand, there is some precedent for similar theories over ocean (Sarachik 1978; Betts and Ridgway 1989; Takahashi 2009). Even accounting for reasonable deviations from RCE, the bound shows that particularly low values of RH are forbidden over ocean, at least in the zonal mean.

5. Explaining the W-shaped latitudinal profile of RH

The theory explains why the latitudinal profile of RH is W-shaped, even though the profiles of specific humidity and saturation specific humidity are not. We provide two different explanations: one in terms of precipitation and net radiation, and the other in terms of soil moisture.

a. Explanation in terms of precipitation and net radiation

We first introduce a simple model linking evaporation to precipitation (P) and net radiation (R_n). Budyko used dimensional analysis to propose the relation $E/P = f(R_n/P)$ (Budyko 1974; Budyko et al. 1980). The relation is valid for averages over sufficiently long time periods, including the steady-state zonal average of interest here. The function linking the two quantities (f) must be determined empirically. A common formulation is $E/P = [1 + (R_n/P)^{-n}]^{-1/n}$, where n is an empirical parameter that typically varies between 1.5 and 2.6, although with some outliers outside this range (Turc 1954; Pike 1964; Choudhury 1999; Yang et al. 2008; Roderick et al. 2014). We adopt the value $n = 2$, consistent with Turc (1954) and Pike (1964), but the following results are not qualitatively sensitive to reasonable variations in this parameter. Dividing both sides by R_n/P yields an expression for the evaporative fraction based on Budyko's relation:

$$EF_B = [1 + (P/R_n)^{-n}]^{-1/n}. \quad (11)$$

The Budyko relation for EF is shown in Fig. 9. Combining Budyko's implied relation for EF with our theory for RH yields a simple explanation for the latitudinal profile of RH in terms of P and R_n . The zonal average profiles of P and R_n (Fig. 10a) imply a profile of P/R_n (Fig. 10b). This quantity has the same units as RH and is qualitatively similar, but is quantitatively inaccurate as a model of RH. For example, it exceeds one in the tropics, and is far too low in the subtropics. As a model of RH, it is also not physically based. Using Eq. (11), the ratio of precipitation to net radiation is converted to an estimate of evaporative fraction (Fig. 10c). The zonal average EF_B is biased low relative to the actual EF estimated from the reanalysis. Nevertheless, it is qualitatively consistent, and captures the W-shaped profile that we seek to explain. Finally, substituting Eq. (11) into Eq. (6) provides an estimate of RH, in terms of P/R_n (Fig. 9). The estimate is reasonably accurate (Fig. 10d), although less so than the prediction derived when using the actual reanalysis EF.

We can now answer the question posed earlier. The reason the nonmonotonic W-shaped profile is present in RH is because it is present in EF, which scales with P/R_n [Eq. (11)]. Our theory quantitatively links zonal mean precipitation to

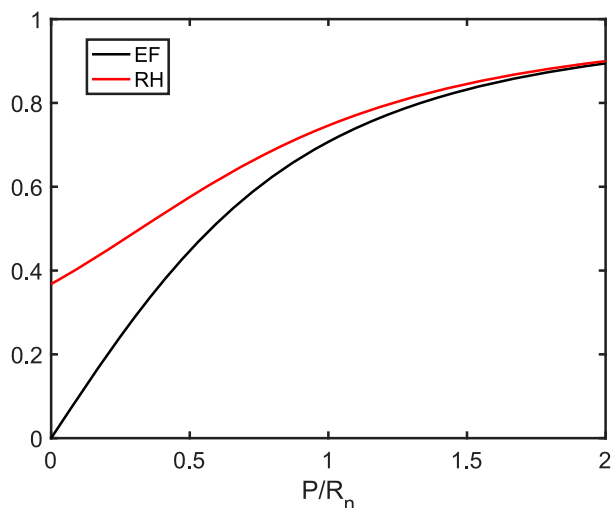


FIG. 9. Budyko's implied relation between EF and P/R_n [Eq. (11), black solid line], and the implied relation between RH and P/R_n [obtained from combining Eqs. (11) and (6), red solid line].

RH via evaporation from the land surface. In contrast, EF is not a substantial control on specific humidity or saturation specific humidity, and thus this pattern is not present in their zonal mean profiles. While there is certainly some land surface impact on these quantities, the zonal mean specific humidity over land is primarily set by advection of moisture from the ocean (e.g., van der Ent and Savenije 2013). Zonal mean saturation specific humidity over land is a function of air temperature, which is primarily determined by net radiation and poleward heat transport (e.g., North et al. 1981).

Note that precipitation alone is not sufficient to explain the latitudinal profile of RH. For example, precipitation is much larger at the equator than anywhere else, whereas RH is not. This is because the sensitivity of EF to P diminishes with increasing P , based on the Budyko curve. Combining Eqs. (11) and (6) (Fig. 9) results in a concave down relation between RH and P/R_n (Fig. 9); since most of the variability in P/R_n arises from variability in P , this implies a concave down relation between RH and P . Thus, the sensitivity of RH to P declines with increasing P , all else being equal. Equivalently, the land surface in the tropics is typically energy-limited rather than water-limited. This explanation relies on properties of the land surface and evaporation, rather than exclusively on atmospheric processes.

b. Explanation in terms of soil moisture

Alternatively, the pattern can be explained in terms of soil moisture using similar arguments to those in the previous section. Soil water storage is a first-order control on evaporation in many regions (Manabe 1969; Budyko 1974; Eagleson 1978), to the extent that EF is often conceptually modeled as a simple increasing function of (normalized) soil moisture s up to some threshold, above which it is constant (e.g., Koster et al. 2009; Seneviratne et al. 2010; Koster and Mahanama 2012).

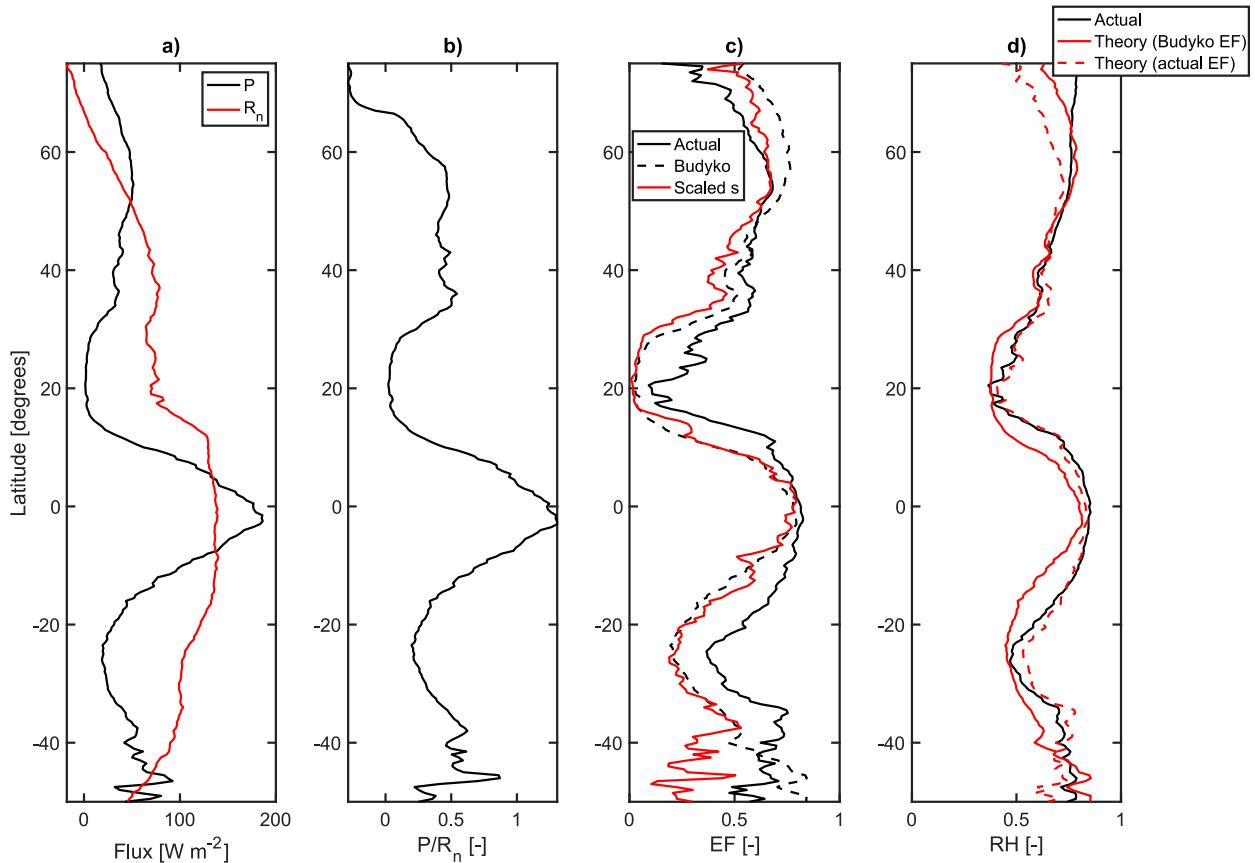


FIG. 10. Zonal median profiles over land of (a) reanalysis precipitation (P) and surface net radiation (R_n), both in units of W m^{-2} ; (b) P/R_n ; (c) EF from the reanalysis (black solid line), Budyko's relation [Eq. (11); black dashed line], and surface (0–7 cm) volumetric soil moisture from the reanalysis, scaled by a factor of 2, to aid comparison with EF (red solid line); (d) RH from the reanalysis (black solid line), Budyko's relation for EF combined with our theory [Eqs. (11) and (6), red solid line], and reanalysis EF combined with our theory [Eq. (6); red dashed line].

Combined with our theory, this information is sufficient to answer the question about the RH profile posed earlier. The parameters of the function linking s and EF typically vary in space, so we do not make a quantitative comparison. However, since the zonal mean profile of soil moisture is W-shaped [Fig. 9c; see also Fig. 2a of McColl et al. (2017)], and since EF scales with soil moisture, our theory implies that RH should also follow a W-shaped profile. From this perspective, the simplest control on RH over land in the current climate is soil moisture.

6. Summary and discussion

We have presented a parsimonious theory of RH over land (where “RH” is shorthand for “zonally and temporally averaged near-surface RH” throughout the article). The theory relates RH to EF by combining two energy budgets: 1) an energy budget of the atmosphere below the LCL, in which surface sensible heating balances diabatic cooling (both radiative cooling and latent cooling from the re-evaporation of falling hydrometeors), and 2) an energy budget of the entire atmospheric column, in which the sum of surface sensible and

latent heat fluxes are balanced by radiative cooling. The theory answers the questions posed in the introduction:

- For the modern Earth, the diabatic cooling rate (the sum of radiative and precipitation re-evaporation cooling rates) below the LCL is typically several times the radiative cooling rate of the entire atmospheric column. Given that, RH is never especially low over land because EF is nonnegative over land, at least for zonal and temporal averages outside high latitudes. RH is never extremely low over ocean because that would violate a lower bound on EF over saturated surfaces (Philip 1987).
- RH inherits the W-shaped zonal mean profile of soil moisture because it scales with EF which, in turn, scales with soil moisture (and P/R_n). In contrast, the W-shaped profile is not present in specific humidity or saturation specific humidity because they are primarily determined by atmospheric mechanisms, and are less tightly constrained by land surface mechanisms. In other words, the theory predicts that the latitudinal profile of RH should look more like that of water stored in the soil than in the air.

The theory's assumptions are most reasonable at large spatial and temporal scales. While we have focused on zonal and multiyear means in this study, the theory may still be skillful at finer spatial and temporal scales. Phenomenological theories that predict EF based on near-surface RH and other near-surface atmospheric measurements have been empirically successful at time scales as short as daily (Salvucci and Gentile 2013; McColl et al. 2019; McColl and Rigden 2020). The connection between those approaches and the theory presented here will be investigated in future work. In addition, we plan to build on previous studies (Byrne and O'Gorman 2016, 2018) to use the theory to better understand how land surface changes mediate changes in RH in a warming world.

Acknowledgments. K.A.M. acknowledges funding from NSF Grant AGS-2129576 and a Sloan Research Fellowship. We thank Dr. Marat Khairoutdinov for providing the models used in this study (SAM and SLM), and Dr. Nick Lutsko for providing code for estimating precipitation re-evaporation from SAM outputs. Thanks to Guido Salvucci and two anonymous reviewers for helpful reviews. The computations in this paper were run on the FASRC Cannon cluster supported by the FAS Division of Science Research Computing Group at Harvard University.

Data availability statement. The datasets generated for this study are available from the corresponding author on request.

APPENDIX A

Derivation of Conceptual Model

We start with a diurnally averaged, horizontally homogeneous boundary layer over land. Neglecting viscous terms (which are typically small), and assuming zero mean vertical flow (consistent with RCE), the enthalpy budget of the boundary layer is

$$\frac{\partial \theta}{\partial t} = -\rho g \frac{\partial \overline{w'\theta'}}{\partial p} + \frac{g}{c_p} \frac{\partial F_R}{\partial p} + \frac{g}{c_p} \frac{\partial F_P}{\partial p}, \quad (\text{A1})$$

where θ is potential temperature, $\overline{w'\theta'}$ is vertical turbulent sensible heat flux, F_R is the net radiative heat flux, and F_P is the flux of energy due to precipitation re-evaporation. For more details, see, for example, section 2.2.4 of Garratt (1994). Averaging this equation in time, and also averaging vertically between the surface and LCL gives

$$\begin{aligned} 0 &= \frac{-\rho g}{p_{\text{LCL}} - p_s} \int_{p_s}^{p_{\text{LCL}}} \frac{\partial \overline{w'\theta'}}{\partial p} dp + \overbrace{\frac{g}{c_p(p_{\text{LCL}} - p_s)} \int_{p_s}^{p_{\text{LCL}}} \frac{\partial F_R}{\partial p} dp}^{\substack{\text{Mean radiative} \\ \text{cooling rate below the LCL} \\ \equiv Q_R(p_{\text{LCL}}) \text{ (K s}^{-1}\text{)}}} + \overbrace{\frac{g}{c_p(p_{\text{LCL}} - p_s)} \int_{p_s}^{p_{\text{LCL}}} \frac{\partial F_P}{\partial p} dp}^{\substack{\text{Mean precipitation} \\ \text{re-evaporation cooling rate} \\ \text{below the LCL} \\ \equiv Q_P(p_{\text{LCL}}) \text{ (K s}^{-1}\text{)}}} \\ &= \frac{-g}{c_p(p_{\text{LCL}} - p_s)} \left\{ \rho c_p \overline{w'\theta'} \Big|_{p=p_{\text{LCL}}} - \underbrace{\rho c_p \overline{w'\theta'} \Big|_{p=p_s}}_{\substack{\text{Surface} \\ \text{sensible heat flux} \\ \equiv H \text{ (W m}^{-2}\text{)}}} - \frac{c_p(p_{\text{LCL}} - p_s)}{g} [Q_R(p_{\text{LCL}}) + Q_P(p_{\text{LCL}})] \right\}. \end{aligned}$$

The turbulent flux at the LCL $\rho c_p \overline{w'\theta'} \Big|_{p=p_{\text{LCL}}}$ is zero if the boundary layer height lies below the LCL height. If the boundary layer height coincides with the LCL height, then the turbulent flux at the LCL height can be nonzero. However, Driedonks (1982) showed that a large majority of the energy entrained into the boundary layer by this flux is used to grow the boundary layer, rather than warm it; thus, it is reasonable to approximate it as zero in the energy budget in this case, too, resulting in Eq. (1).

APPENDIX B

Derivation of Eq. (4) from Eq. (3)

Combining Eqs. (22a)–(22f) of Romps (2017) with Eq. (3) gives

$$\text{EF} = 1 - \beta \left(1 - \left\{ \frac{c}{W_{-1}[\text{RH}^{1/a} c \exp(c)]} \right\}^{c_{pv}/R_a} \right), \quad (\text{B1})$$

where $W_{-1}(\cdot)$ is the negative branch of the Lambert-W function (Corless et al. 1996),

$$a = \frac{c_{pa}}{R_a} + \frac{c_{vl} - c_{pv}}{R_v},$$

$$b = -\frac{E_{0v} - (c_{vv} - c_{vl})T_{\text{trip}}}{R_v T_a} \approx -\frac{E_{0v} - (c_{vv} - c_{vl})T_{\text{trip}}}{R_v T_0},$$

$$c = b/a,$$

and all other terms are constants defined in Table 1. We have made two approximations to the original equations presented in Romps (2017). First, the specific gas constant of moist air

(R_m) and the specific heat capacity of moist air at constant pressure (c_{pm}) are replaced with their dry air equivalents (R_a and c_{pa} , respectively). Second, in the expression for b , we replace the near-surface air temperature in the denominator with a constant reference temperature (T_0). Errors induced by these approximations are small compared with other approximations made in the derivation.

Rearranging to solve for RH yields

$$\text{RH} = \left\{ \left(1 - \frac{1 - \text{EF}}{\beta} \right)^{-R_a/c_{pa}} \exp \left[c \left(1 - \frac{1 - \text{EF}}{\beta} \right)^{-R_a/c_{pa}} - c \right] \right\}^a. \quad (\text{B2})$$

These equations can be further simplified by linearizing around a reference state. While we could simply linearize Eq. (B1) around $\text{RH} = 1$, the function is nonlinear (Fig. 5), and the resulting linear approximation becomes quite inaccurate for lower RH. However, the relation between EF and $\log(\text{RH})$ appears quasi-linear (not shown). Thus, if we instead define $x = \log(\text{RH})$, substitute it into Eq. (B1) and linearize around $x = 0$, the resulting approximation is quantitatively more accurate. Specifically, we obtain

$$\begin{aligned} \text{EF} &= 1 - \beta \left[1 - \left(\frac{c}{W_{-1} \{ [\exp(x)]^{1/a} c \exp(c) \}} \right)^{c_{pa}/R_a} \right] \equiv f(x) \\ &\approx f(0) + f'(0)x \\ &= 1 - \beta \left(1 - \left\{ \frac{c}{W_{-1} [c \exp(c)]} \right\}^{c_{pa}/R_a} \right) \\ &\quad - \frac{\beta c_{pa} \left\{ \frac{c}{W_{-1} [c \exp(c)]} \right\}^{c_{pa}/R_a}}{a R_a \{ 1 + W_{-1} [c \exp(c)] \}} x \end{aligned}$$

where we have used the relation $W'_{-1}(x) = W_{-1}(x)/\{x[1 + W_{-1}(x)]\}$. Finally, applying the identity $W_{-1}[c \exp(c)] = c$ results in Eq. (4), where α is defined as

$$\alpha \equiv \frac{c_{pa}}{a R_a} \left(\frac{-1}{1 + c} \right). \quad (\text{B3})$$

APPENDIX C

Philip's Bound on the Evaporative Fraction over a Saturated Surface

In this appendix, we review the derivation of the lower bound on the evaporative fraction over a saturated surface proposed in Philip (1987). The sensible and latent heat fluxes from the surface are

$$H = -\rho c_p K \frac{\partial T}{\partial z} \Big|_{z=0}, \quad (\text{C1})$$

$$\lambda E = -\rho \lambda K \frac{\partial q}{\partial z} \Big|_{z=0}, \quad (\text{C2})$$

where K is a turbulent diffusivity, and can be taken as equal for both sensible and latent heat fluxes. The Bowen ratio is thus

$$\frac{H}{\lambda E} = \frac{c_p}{\lambda \frac{\partial q}{\partial T} \Big|_{T=T_s}}, \quad (\text{C3})$$

where $T_s = T(0)$. For a saturated surface, the specific humidity at the surface is equal to the saturation specific humidity. Thus, at some point z sufficiently close to the surface, we have

$$q(z) = q^*(T_s) + \frac{\partial q}{\partial T} \Big|_{T=T_s} \frac{\partial T}{\partial z} \Big|_{z=0} z, \quad (\text{C4})$$

$$q^*(z) = q^*(T_s) + \frac{\partial q^*}{\partial T} \Big|_{T=T_s} \frac{\partial T}{\partial z} \Big|_{z=0} z. \quad (\text{C5})$$

Supersaturation is forbidden, which requires that $q(z) \leq q^*(z)$ for any z and thus

$$\frac{\partial q}{\partial T} \Big|_{T=T_s} \frac{\partial T}{\partial z} \Big|_{z=0} \leq \frac{\partial q^*}{\partial T} \Big|_{T=T_s} \frac{\partial T}{\partial z} \Big|_{z=0}. \quad (\text{C6})$$

Assuming $H > 0$ and thus $\partial T/\partial z|_{z=0} < 0$, as is common over land, implies that

$$\frac{\partial q}{\partial T} \Big|_{T=T_s} \geq \frac{\partial q^*}{\partial T} \Big|_{T=T_s}. \quad (\text{C7})$$

While H is not always positive, particularly at night over land, it is consistently positive in the zonal mean in the reanalysis over land and ocean, justifying this assumption. Substituting this relation into Eq. (C3), and using the identity $\text{EF} = (1 + H/\lambda E)^{-1}$ yields the inequality

$$\text{EF} \geq \frac{\frac{\lambda \partial q^*}{c_p \partial T} \Big|_{T=T_s}}{\frac{\lambda \partial q^*}{c_p \partial T} \Big|_{T=T_s} + 1}. \quad (\text{C8})$$

Combining this with the Clausius-Clapeyron relation

$$\frac{\partial q^*}{\partial T} = \frac{\lambda q^*}{R_v T^2}, \quad (\text{C9})$$

and the fact that near-surface air temperature T_a must be less than T_s due to the negative temperature gradient, results in Eq. (9).

REFERENCES

- Allen, M. R., and W. J. Ingram, 2002: Constraints on future changes in climate and the hydrologic cycle. *Nature*, **419**, 224–232, <https://doi.org/10.1038/nature01092>.
- Andrews, T., M. Doutriaux-Boucher, O. Boucher, and P. M. Forster, 2011: A regional and global analysis of carbon dioxide physiological forcing and its impact on climate. *Climate Dyn.*, **36**, 783–792, <https://doi.org/10.1007/s00382-010-0742-1>.
- Becker, T., and B. Stevens, 2014: Climate and climate sensitivity to changing CO₂ on an idealized land planet. *J. Adv. Model. Earth Syst.*, **6**, 1205–1223, <https://doi.org/10.1002/2014MS000369>.

- Berg, A., and Coauthors, 2016: Land–atmosphere feedbacks amplify aridity increase over land under global warming. *Nat. Climate Change*, **6**, 869–874, <https://doi.org/10.1038/nclimate3029>.
- Berry, J. A., D. J. Beerling, and P. J. Franks, 2010: Stomata: Key players in the Earth system, past and present. *Curr. Opin. Plant Biol.*, **13**, 232–239, <https://doi.org/10.1016/j.pbi.2010.04.013>.
- Betts, A. K., 1994: Relation between equilibrium evaporation and the saturation pressure budget. *Bound.-Layer Meteor.*, **71**, 235–245, <https://doi.org/10.1007/BF00713740>.
- , 2000: Idealized model for equilibrium boundary layer over land. *J. Hydrometeor.*, **1**, 507–523, [https://doi.org/10.1175/1525-7541\(2000\)001<0507:IMFEBL>2.0.CO;2](https://doi.org/10.1175/1525-7541(2000)001<0507:IMFEBL>2.0.CO;2).
- , and W. Ridgway, 1989: Climatic equilibrium of the atmospheric convective boundary layer over a tropical ocean. *J. Atmos. Sci.*, **46**, 2621–2641, [https://doi.org/10.1175/1520-0469\(1989\)046<2621:CEOTAC>2.0.CO;2](https://doi.org/10.1175/1520-0469(1989)046<2621:CEOTAC>2.0.CO;2).
- Beucler, T., and T. W. Cronin, 2016: Moisture-radiative cooling instability. *J. Adv. Model. Earth Syst.*, **8**, 1620–1640, <https://doi.org/10.1002/2016MS000763>.
- Brubaker, K. L., and D. Entekhabi, 1995: An analytic approach to modeling land-atmosphere interaction: 1. Construct and equilibrium behavior. *Water Resour. Res.*, **31**, 619–632, <https://doi.org/10.1029/94WR01772>.
- , and —, 1996: Analysis of feedback mechanisms in land-atmosphere interaction. *Water Resour. Res.*, **32**, 1343–1357, <https://doi.org/10.1029/96WR00005>.
- Budyko, M. I., 1974: *Climate and Life*. Academic Press, 508 pp.
- , T. G. Berlyand, N. A. Yefimova, L. I. Zubenok, and L. A. Strokinina, 1980: Heat balance of the earth. NASA-TM-75826, 52 pp., <https://ntrs.nasa.gov/search.jsp?R=19810004876>.
- Buzan, J. R., and M. Huber, 2020: Moist heat stress on a hotter earth. *Annu. Rev. Earth Planet. Sci.*, **48**, 623–655, <https://doi.org/10.1146/annurev-earth-053018-060100>.
- Byrne, M. P., and P. A. O’Gorman, 2016: Understanding decreases in land relative humidity with global warming: Conceptual model and GCM simulations. *J. Climate*, **29**, 9045–9061, <https://doi.org/10.1175/JCLI-D-16-0351.1>.
- , and —, 2018: Trends in continental temperature and humidity directly linked to ocean warming. *Proc. Natl. Acad. Sci. USA*, **115**, 4863–4868, <https://doi.org/10.1073/pnas.1722312115>.
- Cao, L., G. Bala, K. Caldeira, R. Nemani, and G. Ban-Weiss, 2010: Importance of carbon dioxide physiological forcing to future climate change. *Proc. Natl. Acad. Sci. USA*, **107**, 9513–9518, <https://doi.org/10.1073/pnas.0913000107>.
- Choudhury, B., 1999: Evaluation of an empirical equation for annual evaporation using field observations and results from a biophysical model. *J. Hydrol.*, **216**, 99–110, [https://doi.org/10.1016/S0022-1694\(98\)00293-5](https://doi.org/10.1016/S0022-1694(98)00293-5).
- Corless, R. M., G. H. Gonnet, D. E. G. Hare, D. J. Jeffrey, and D. E. Knuth, 1996: On the Lambert W function. *Adv. Comput. Math.*, **5**, 329–359, <https://doi.org/10.1007/BF02124750>.
- Delworth, T., and S. Manabe, 1989: The influence of soil wetness on near-surface atmospheric variability. *J. Climate*, **2**, 1447–1462, [https://doi.org/10.1175/1520-0442\(1989\)002<1447:TIOSWO>2.0.CO;2](https://doi.org/10.1175/1520-0442(1989)002<1447:TIOSWO>2.0.CO;2).
- Dessler, A. E., and S. C. Sherwood, 2000: Simulations of tropical upper tropospheric humidity. *J. Geophys. Res.*, **105**, 20155–20163, <https://doi.org/10.1029/2000JD900231>.
- Driedonks, A. G. M., 1982: Sensitivity analysis of the equations for a convective mixed layer. *Bound.-Layer Meteor.*, **22**, 475–480, <https://doi.org/10.1007/BF00124706>.
- Eagleson, P. S., 1978: Climate, soil, and vegetation: 4. The expected value of annual evapotranspiration. *Water Resour. Res.*, **14**, 731–739, <https://doi.org/10.1029/WR014i005p00731>.
- Entekhabi, D., and K. L. Brubaker, 1995: An analytic approach to modeling land–atmosphere interaction: 2. Stochastic formulation. *Water Resour. Res.*, **31**, 633–643, <https://doi.org/10.1029/94WR01773>.
- Fildier, B., C. Muller, R. Pincus, and S. Fueglistaler, 2023: How moisture shapes low-level radiative cooling in subsidence regimes. *AGU Adv.*, **4**, e2023AV000880, <https://doi.org/10.1029/2023AV000880>.
- Frierson, D. M. W., I. M. Held, and P. Zurita-Gotor, 2006: A gray-radiation aquaplanet moist GCM. Part I: Static stability and eddy scale. *J. Atmos. Sci.*, **63**, 2548–2566, <https://doi.org/10.1175/JAS3753.1>.
- Garratt, J. R., 1994: *The Atmospheric Boundary Layer*. Cambridge University Press, 336 pp.
- Gentine, P., G.-J. Steeneveld, B. G. Heusinkveld, and A. A. M. Holtslag, 2018: Coupling between radiative flux divergence and turbulence near the surface. *Quart. J. Roy. Meteor. Soc.*, **144**, 2491–2507, <https://doi.org/10.1002/qj.3333>.
- Ha, K.-J., and L. Mahrt, 2003: Radiative and turbulent fluxes in the nocturnal boundary layer. *Tellus*, **55A**, 317–327, <https://doi.org/10.3402/tellusa.v55i4.12103>.
- Held, I. M., and B. J. Soden, 2000: Water vapor feedback and global warming. *Annu. Rev. Energy Environ.*, **25**, 441–475, <https://doi.org/10.1146/annurev.energy.25.1.441>.
- Hersbach, H., and Coauthors, 2020: The ERA5 global reanalysis. *Quart. J. Roy. Meteor. Soc.*, **146**, 1999–2049, <https://doi.org/10.1002/qj.3803>.
- Jeevanjee, N., and D. M. Romps, 2018: Mean precipitation change from a deepening troposphere. *Proc. Natl. Acad. Sci. USA*, **115**, 11465–11470, <https://doi.org/10.1073/pnas.1720683115>.
- , and S. Fueglistaler, 2020: On the cooling-to-space approximation. *J. Atmos. Sci.*, **77**, 465–478, <https://doi.org/10.1175/JAS-D-18-0352.1>.
- , and L. Zhou, 2022: On the resolution-dependence of anvil cloud fraction and precipitation efficiency in radiative-convective equilibrium. *J. Adv. Model. Earth Syst.*, **14**, e2021MS002759, <https://doi.org/10.1029/2021MS002759>.
- Khairoutdinov, M. F., and D. A. Randall, 2003: Cloud resolving modeling of the ARM summer 1997 IOP: Model formulation, results, uncertainties, and sensitivities. *J. Atmos. Sci.*, **60**, 607–625, [https://doi.org/10.1175/1520-0469\(2003\)060<0607:CRMOTA>2.0.CO;2](https://doi.org/10.1175/1520-0469(2003)060<0607:CRMOTA>2.0.CO;2).
- Kim, C. P., and D. Entekhabi, 1998: Feedbacks in the land-surface and mixed-layer energy budgets. *Bound.-Layer Meteor.*, **88** (1), 1–21, <https://doi.org/10.1023/A:1001094008513>.
- Kodama, T., A. Nitta, H. Genda, Y. Takao, R. O’ishi, A. Abe-Ouchi, and Y. Abe, 2018: Dependence of the onset of the runaway greenhouse effect on the latitudinal surface water distribution of earth-like planets. *J. Geophys. Res. Planets*, **123**, 559–574, <https://doi.org/10.1002/2017JE005383>.
- Koster, R. D., and S. P. P. Mahanama, 2012: Land surface controls on hydroclimatic means and variability. *J. Hydrometeor.*, **13**, 1604–1620, <https://doi.org/10.1175/JHM-D-12-050.1>.
- , S. D. Schubert, and M. J. Suarez, 2009: Analyzing the concurrence of meteorological droughts and warm periods, with implications for the determination of evaporative regime. *J. Climate*, **22**, 3331–3341, <https://doi.org/10.1175/2008JCLI2718.1>.
- Krakauer, N. Y., B. I. Cook, and M. J. Puma, 2010: Contribution of soil moisture feedback to hydroclimatic variability. *Hydrol. Earth Syst. Sci.*, **14**, 505–520, <https://doi.org/10.5194/hess-14-505-2010>.

- Laguë, M. M., G. R. Quetin, and W. R. Boos, 2023: Reduced terrestrial evaporation increases atmospheric water vapor by generating cloud feedbacks. *Environ. Res. Lett.*, **18**, 074021, <https://doi.org/10.1088/1748-9326/acdabe>.
- Lee, J. M., and M. Khairoutdinov, 2015: A Simplified Land Model (SLM) for use in cloud-resolving models: Formulation and evaluation. *J. Adv. Model. Earth Syst.*, **7**, 1368–1392, <https://doi.org/10.1002/2014MS000419>.
- Lutsko, N. J., and T. W. Cronin, 2018: Increase in precipitation efficiency with surface warming in radiative-convective equilibrium. *J. Adv. Model. Earth Syst.*, **10**, 2992–3010, <https://doi.org/10.1029/2018MS001482>.
- Maes, W. H., P. Gentine, N. E. C. Verhoest, and D. G. Miralles, 2019: Potential evaporation at eddy-covariance sites across the globe. *Hydrol. Earth Syst. Sci.*, **23**, 925–948, <https://doi.org/10.5194/hess-23-925-2019>.
- Manabe, S., 1969: Climate and the ocean circulation. *Mon. Wea. Rev.*, **97**, 739–774, [https://doi.org/10.1175/1520-0493\(1969\)097<0739:CATOC>2.3.CO;2](https://doi.org/10.1175/1520-0493(1969)097<0739:CATOC>2.3.CO;2).
- McColl, K. A., and A. J. Rigden, 2020: Emergent simplicity of continental evapotranspiration. *Geophys. Res. Lett.*, **47**, e2020GL087101, <https://doi.org/10.1029/2020GL087101>.
- , S. H. Alemohammad, R. Akbar, A. G. Konings, S. Yueh, and D. Entekhabi, 2017: The global distribution and dynamics of surface soil moisture. *Nat. Geosci.*, **10**, 100–104, <https://doi.org/10.1038/ngeo2868>.
- , G. D. Salvucci, and P. Gentine, 2019: Surface flux equilibrium theory explains an empirical estimate of water-limited daily evapotranspiration. *J. Adv. Model. Earth Syst.*, **11**, 2036–2049, <https://doi.org/10.1029/2019MS001685>.
- McNaughton, K. G., 1976a: Evaporation and advection I: Evaporation from extensive homogeneous surfaces. *Quart. J. Roy. Meteor. Soc.*, **102**, 181–191, <https://doi.org/10.1002/qj.49710243115>.
- , 1976b: Evaporation and advection II: Evaporation downwind of a boundary separating regions having different surface resistances and available energies. *Quart. J. Roy. Meteor. Soc.*, **102**, 193–202, <https://doi.org/10.1002/qj.49710243116>.
- Milly, P. C. D., and K. A. Dunne, 2016: Potential evapotranspiration and continental drying. *Nat. Climate Change*, **6**, 946–949, <https://doi.org/10.1038/nclimate3046>.
- Miyawaki, O., T. A. Shaw, and M. F. Jansen, 2022: Quantifying energy balance regimes in the modern climate, their link to lapse rate regimes, and their response to warming. *J. Climate*, **35**, 1045–1061, <https://doi.org/10.1175/JCLI-D-21-0440.1>.
- Neelin, J. D., and I. M. Held, 1987: Modeling tropical convergence based on the moist static energy budget. *Mon. Wea. Rev.*, **115**, 3–12, [https://doi.org/10.1175/1520-0493\(1987\)115<0003:MTCBOT>2.0.CO;2](https://doi.org/10.1175/1520-0493(1987)115<0003:MTCBOT>2.0.CO;2).
- North, G. R., R. F. Cahalan, and J. A. Coakley Jr., 1981: Energy balance climate models. *Rev. Geophys.*, **19**, 91–121, <https://doi.org/10.1029/RG019i001p00091>.
- O’Gorman, P. A., and T. Schneider, 2008: The hydrological cycle over a wide range of climates simulated with an idealized GCM. *J. Climate*, **21**, 3815–3832, <https://doi.org/10.1175/2007JCLI2065.1>.
- , N. Lamquin, T. Schneider, and M. S. Singh, 2011: The relative humidity in an isentropic advection–condensation model: Limited poleward influence and properties of subtropical minima. *J. Atmos. Sci.*, **68**, 3079–3093, <https://doi.org/10.1175/JAS-D-11-067.1>.
- , R. P. Allan, M. P. Byrne, and M. Previdi, 2012: Energetic constraints on precipitation under climate change. *Surv. Geophys.*, **33**, 585–608, <https://doi.org/10.1007/s10712-011-9159-6>.
- Philip, J. R., 1987: A physical bound on the Bowen ratio. *J. Climate Appl. Meteor.*, **26**, 1043–1045, [https://doi.org/10.1175/1520-0450\(1987\)026<1043:APBOTB>2.0.CO;2](https://doi.org/10.1175/1520-0450(1987)026<1043:APBOTB>2.0.CO;2).
- Pierrehumbert, R. T., 2010: *Principles of Planetary Climate*. Cambridge University Press, 679 pp.
- , and R. Roca, 1998: Evidence for control of Atlantic subtropical humidity by large scale advection. *Geophys. Res. Lett.*, **25**, 4537–4540, <https://doi.org/10.1029/1998GL900203>.
- , H. Brogniez, and R. Roca, 2008: On the relative humidity of the atmosphere. *The Global Circulation of the Atmosphere*, T. Schneider and A. H. Sobel, Eds., Princeton University Press, 143–185.
- Pike, J. G., 1964: The estimation of annual run-off from meteorological data in a tropical climate. *J. Hydrol.*, **2**, 116–123, [https://doi.org/10.1016/0022-1694\(64\)90022-8](https://doi.org/10.1016/0022-1694(64)90022-8).
- Priestley, C. H. B., and R. J. Taylor, 1972: On the assessment of surface heat flux and evaporation using large-scale parameters. *Mon. Wea. Rev.*, **100**, 81–92, [https://doi.org/10.1175/1520-0493\(1972\)100<0081:OTAOSH>2.3.CO;2](https://doi.org/10.1175/1520-0493(1972)100<0081:OTAOSH>2.3.CO;2).
- Raupach, M. R., 2001: Combination theory and equilibrium evaporation. *Quart. J. Roy. Meteor. Soc.*, **127**, 1149–1181, <https://doi.org/10.1002/qj.49712757402>.
- Roderick, M. L., F. Sun, W. H. Lim, and G. D. Farquhar, 2014: A general framework for understanding the response of the water cycle to global warming over land and ocean. *Hydrol. Earth Syst. Sci.*, **18**, 1575–1589, <https://doi.org/10.5194/hess-18-1575-2014>.
- Romps, D. M., 2014: An analytical model for tropical relative humidity. *J. Climate*, **27**, 7432–7449, <https://doi.org/10.1175/JCLI-D-14-00255.1>.
- , 2017: Exact expression for the lifting condensation level. *J. Atmos. Sci.*, **74**, 3891–3900, <https://doi.org/10.1175/JAS-D-17-0102.1>.
- Salvucci, G. D., and P. Gentine, 2013: Emergent relation between surface vapor conductance and relative humidity profiles yields evaporation rates from weather data. *Proc. Natl. Acad. Sci. USA*, **110**, 6287–6291, <https://doi.org/10.1073/pnas.1215844110>.
- Sarachik, E. S., 1978: Tropical sea surface temperature: An interactive one-dimensional atmosphere–ocean model. *Dyn. Atmos. Oceans*, **2**, 455–469, [https://doi.org/10.1016/0377-0265\(78\)90014-3](https://doi.org/10.1016/0377-0265(78)90014-3).
- , 1985: A simple theory for the vertical structure of the tropical atmosphere. *Pure Appl. Geophys.*, **123**, 261–271, <https://doi.org/10.1007/BF00877022>.
- Schneider, T., P. A. O’Gorman, and X. J. Levine, 2010: Water vapor and the dynamics of climate changes. *Rev. Geophys.*, **48**, RG3001, <https://doi.org/10.1029/2009RG000302>.
- Seneviratne, S. I., T. Corti, E. L. Davin, M. Hirschi, E. B. Jaeger, I. Lehner, B. Orlowsky, and A. J. Teuling, 2010: Investigating soil moisture–climate interactions in a changing climate: A review. *Earth Sci. Rev.*, **99**, 125–161, <https://doi.org/10.1016/j.earscirev.2010.02.004>.
- Sherwood, S. C., 1996: Maintenance of the free-tropospheric tropical water vapor distribution. Part II: Simulation by large-scale advection. *J. Climate*, **9**, 2919–2934, [https://doi.org/10.1175/1520-0442\(1996\)009<2919:MOTFTT>2.0.CO;2](https://doi.org/10.1175/1520-0442(1996)009<2919:MOTFTT>2.0.CO;2).
- , and C. L. Meyer, 2006: The general circulation and robust relative humidity. *J. Climate*, **19**, 6278–6290, <https://doi.org/10.1175/JCLI3979.1>.
- , E. R. Kursinski, and W. G. Read, 2006: A distribution law for free-tropospheric relative humidity. *J. Climate*, **19**, 6267–6277, <https://doi.org/10.1175/JCLI3978.1>.
- , W. Ingram, Y. Tsushima, M. Satoh, M. Roberts, P. L. Vidale, and P. A. O’Gorman, 2010a: Relative humidity changes in a

- warmer climate. *J. Geophys. Res.*, **115**, D09104, <https://doi.org/10.1029/2009JD012585>.
- , R. Roca, T. M. Weckwerth, and N. G. Andronova, 2010b: Tropospheric water vapor, convection, and climate. *Rev. Geophys.*, **48**, RG2001, <https://doi.org/10.1029/2009RG000301>.
- Singh, M. S., R. A. Warren, and C. Jakob, 2019: A steady-state model for the relationship between humidity, instability, and precipitation in the tropics. *J. Adv. Model. Earth Syst.*, **11**, 3973–3994, <https://doi.org/10.1029/2019MS001686>.
- Slatyer, R. O., and I. C. McIlroy, 1961: *Practical Microclimatology, with Special Reference to the Water Factor in Soil–Plant–Atmosphere Relationships*. Commonwealth Scientific and Industrial Research Organisation, 307 pp., <https://www.cabdirect.org/cabdirect/abstract/19621702167>.
- Swann, A. L. S., F. M. Hoffman, C. D. Koven, and J. T. Rander-son, 2016: Plant responses to increasing CO₂ reduce estimates of climate impacts on drought severity. *Proc. Natl. Acad. Sci. USA*, **113**, 10019–10024, <https://doi.org/10.1073/pnas.1604581113>.
- Takahashi, K., 2009: Radiative constraints on the hydrological cycle in an idealized radiative–convective equilibrium model. *J. Atmos. Sci.*, **66**, 77–91, <https://doi.org/10.1175/2008JAS2797.1>.
- Turc, L., 1954: Le bilan d'eau des sols: Relations entre les précipitations, l'évaporation et l'écoulement. *J. Hydr.*, **5**, 36–44.
- van der Ent, R. J., and H. H. G. Savenije, 2013: Oceanic sources of continental precipitation and the correlation with sea surface temperature. *Water Resour. Res.*, **49**, 3993–4004, <https://doi.org/10.1002/wrcr.20296>.
- Yang, H., D. Yang, Z. Lei, and F. Sun, 2008: New analytical derivation of the mean annual water-energy balance equation. *Water Resour. Res.*, **44**, W03410, <https://doi.org/10.1029/2007WR006135>.
- Yin, J., J. D. Albertson, J. R. Rigby, and A. Porporato, 2015: Land and atmospheric controls on initiation and intensity of moist convection: CAPE dynamics and LCL crossings. *Water Resour. Res.*, **51**, 8476–8493, <https://doi.org/10.1002/2015WR017286>.
- Zhou, W., L. R. Leung, and J. Lu, 2023: The role of interactive soil moisture in land drying under anthropogenic warming. *Geophys. Res. Lett.*, **50**, e2023GL105308, <https://doi.org/10.1029/2023GL105308>.